Provided for non-commercial research and educational use.
Not for reproduction, distribution or commercial use.

This article was originally published in the *Comprehensive Inorganic Chemistry II*, published by Elsevier, and the attached copy is provided by Elsevier for the author's benefit and for the benefit of the author's institution, for non-commercial research and educational use including without limitation use in instruction at your institution, sending it to specific colleagues who you know, and providing a copy to your institution's administrator.

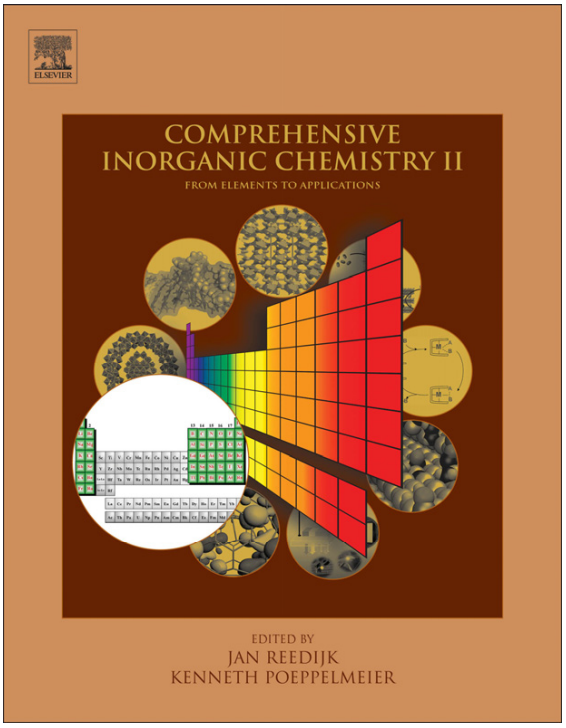

All other uses, reproduction and distribution, including without limitation commercial reprints, selling or licensing copies or access, or posting on open internet sites, your personal or institution's website or repository, are prohibited. For exceptions, permission may be sought for such use through Elsevier's permissions site at:

http://www.elsevier.com/locate/permissionusematerial

Hutin M., Rosnes M.H., Long D.-L. and Cronin L. Polyoxometalates: Synthesis and Structure – From Building Blocks to Emergent Materials. In: Jan Reedijk and Kenneth Poeppelmeier, editors. Comprehensive Inorganic Chemistry II, Vol 2. Oxford: Elsevier; 2013. p. 241-269.

Author's personal copy

2.10 Polyoxometalates: Synthesis and Structure – From Building Blocks to Emergent Materials

M Hutin, MH Rosnes, D-L Long, and L Cronin, University of Glasgow, Glasgow, UK

© 2013 Elsevier Ltd. All rights reserved.

2.10.1	**Introduction**	241
2.10.1.1	History	242
2.10.1.2	Classification	242
2.10.1.3	Synthesis and Assembly	245
2.10.2	**Crystal Engineering by Cation Control**	245
2.10.3	**Nonconventional and Chiral POMs**	246
2.10.3.1	Polyoxoniobates	246
2.10.3.2	Uranium	247
2.10.3.3	Palladium	247
2.10.3.4	Peroxide Ligands	247
2.10.3.5	Chirality	248
2.10.3.6	Oxothiometalates	249
2.10.4	**Mo-Blue and Mo-Brown**	249
2.10.5	**Analytical Tools**	250
2.10.5.1	Mass Spectrometry	250
2.10.5.1.1	ESI-MS and CSI-MS	250
2.10.5.1.2	IMS-MS	252
2.10.5.2	Electrophoresis	252
2.10.5.3	Surface Analysis	253
2.10.6	**POM–Organic Hybrids**	253
2.10.7	**Frameworks**	254
2.10.7.1	POM-Based Frameworks	255
2.10.7.1.1	Silver as the transition-metal linker	255
2.10.7.1.2	Nonsilver-based frameworks	256
2.10.7.1.3	Hybrid frameworks	257
2.10.7.2	POM–MOFs	258
2.10.8	**Redox-Active POMs**	258
2.10.9	**Devices, Catalysts, and Magnetism**	259
2.10.9.1	Catalysis	259
2.10.9.1.1	Water splitting	259
2.10.9.1.2	Catalysts	260
2.10.9.2	Magnetism	261
2.10.10	**POM-Based Emergent Materials**	261
2.10.10.1	Nanostructures by Cation Exchange	263
2.10.10.1.1	Tube growth at a solid–liquid interface	263
2.10.10.1.2	Membrane growth at a liquid–liquid interface	264
2.10.10.2	Soluble Colloids	265
2.10.10.3	Hybrid-Based Nanostructures	265
2.10.10.3.1	Formation of vesicles	265
2.10.10.3.2	Surface studies	265
2.10.11	**Conclusion**	266
References		267

2.10.1 Introduction

Polyoxometalates (POMs) can be described as metal-oxo cluster anions, which cover a large range of structures in terms of size and elemental composition. The terminal oxo-ligands are strong π-electron donors; therefore lone oxygen atoms bind very strongly to main-group transition-metal ions in high oxidation state (principally those in groups V and VI). The ability of hydroxide complexes of molybdenum(VI), tungsten (VI), and vanadium(V) to undergo condensation reactions under acidic conditions is a unique and remarkable property of this class of compounds, and it has sparked a tremendous amount of scientific research ranging from first-principles studies[1,2] to industrial applications.[3]

*Comprehensive Inorganic Chemistry II: From Elements to Applications, (*2013), vol. 2, pp. 241-269

Author's personal copy

2.10.1.1 History

As early as 1826 it was noted by Berzelius that the reaction of ammonium molybdate, $(NH_4)_2MoO_4$, with an excess of phosphoric acid leads to the formation of a light yellow crystalline solid.[4] Following these initial reports, several leading scientists among them Pauling and Werner investigated these molybdates and related tungsten-based compounds in an attempt to understand the structure and composition of the material.[5–7] It required yet another major scientific breakthrough to fully elucidate the nature of the reaction product, namely, crystal structure determination by x-ray diffraction methods, first discovered by Laue in 1912[8] and pioneered by Bragg and Bragg.[9] This method finally allowed the unambiguous identification and structural characterization of the cluster compound: In 1933, Keggin reported the structure of 12-phosphotungstic acid, which was solved by the interpretation of powder-x-ray diffraction images.[10,11]

It has often been said that the molecules encompassed within the area of POM cluster chemistry possess an unmatched range of physical and chemical properties, as well as a set of transferable building blocks that can be reliably utilized in the formation of new materials. These key features are being exploited rapidly after a rise in popularity of POMs, which started in the early 1990s as a result of a key review by Pope and Müller[12] in 1991, which foresaw the present interest. The vast growth and ever-expanding range of applications were also documented in 1998 when Craig Hill organized a special thematic issue in Chemical Reviews, which presented the history, developments, and application of the many areas covered by POM chemistry.[13]

Today, POM chemistry is a key emerging area with the potential to develop sophisticated designer molecule-based materials and devices that bridge several length scales, exploiting the progress made in instrumentation, nanoscale science, and material fabrication methods. In terms of technique development, fast and routine single crystal x-ray diffraction data collection has allowed the number of new structures within the area to accelerate to the point that the bottleneck has moved to structure refinement, or crystallization of new compounds, rather than the time taken for data collection and initial structure solution. There are over 500 papers (not including patents) published each year on POM-related topics, see **Figure 1**. There are numerous reviews addressing different aspects of POM science including new structures, analytical methods, biomedical applications, catalysis, theoretical calculations, as well as perspectives for new materials.[2,14–17]

Here, the aim is not only to present a snapshot of the recent developments in terms of design, architecture, and application of POMs, but also to provide a guide to POMs and their chemistry. The focus is on the multifunctionality of POMs, and how the cluster templates, resulting building blocks, substructures, and overall cluster architectures need to be manipulated at every level to produce hierarchical functional molecular-cluster-based materials, as well as to link together new areas and possible new avenues for POM chemistry and applications. In particular, the emphasis is on POM systems that have potential to present a hierarchy of properties that may be successively 'designed-in' to make highly sophisticated materials.

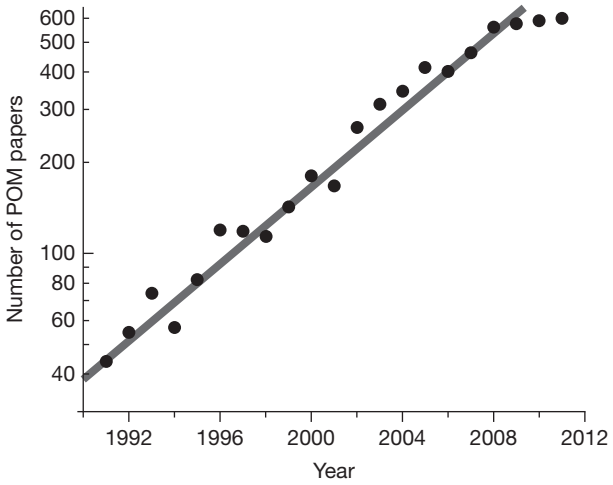

Figure 1 Number of publications involving the study of polyoxometalates plotted against year, on a logarithmic scale. Data obtained from the Web of Science, topic search 'polyoxometal*', from 1990 to 2011, journal and letter entries only.

2.10.1.2 Classification

There is an immense number of compounds that fall under the POM category, which come in a vast range of shapes and sizes with a seemingly endless number of structure types. Therefore, understanding the relationships between the different cluster types can be bewildering. It is possible to broadly classify POMs, helping to conceptualize and understand the many structural types. This classification has limitations and exceptions, but it gives an overview linking the main building block types, structure types, and physical properties. In general, the class of compounds known as POMs is based upon metal-oxide building blocks $\{MO_x\}$ where M (the addenda atom) most commonly is Mo, W, or V, and x is between 4 and 7.[12,18] The initial step in the formation of POMs is the expansion from a tetrahedral hydroxide metal complex to an octahedral hydroxide/oxo metal complex,[19] which next undergoes condensation reactions under acidic conditions, see **Figure 2**.

Nearly all POM clusters are anionic and can thus be complexed with additional cations, known as heteroatoms. The nature of the heteroatom does not show the same restrictions as the addendum atom and is commonly an element with a coordination number of 4, 6, 8, or 12.[20] The heteroatom can be either primary and/or secondary. A primary heteroatom is essential to the POM structure, but does not necessarily need to be located at the center of the POM anion. Lacunary structures, polyanions formed by partial decomposition of their parent compounds, have external vacancies which can be filled by additional cations, known as secondary heteroatoms. These cations, or heteroatoms, can be used to further link the POM structures into larger aggregates. **Figure 3** presents a classification of the POM formulas that are currently known and also shows how the structures relate to each other within a 'polyoxometalate periodic table.'[2] The table tries to summarize and classify the different cluster types and to show the 'link' between the various structures.

Author's personal copy

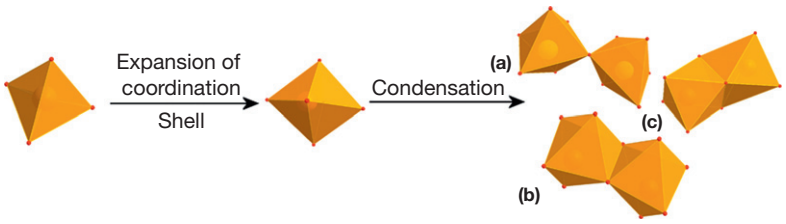

Figure 2 Illustration of the self-assembly process, whereby the tetrahedral metal $\{MO_4\}$ expands into octahedra $\{MO_6\}$ and then condenses into larger assemblies sharing oxygen ligands, where M commonly is Mo, W, or V. There are three different sharing modes: (a) corner sharing, (b) edge sharing, and less commonly (c) face sharing. Color scheme: M, gold (polyhedra); O, red.

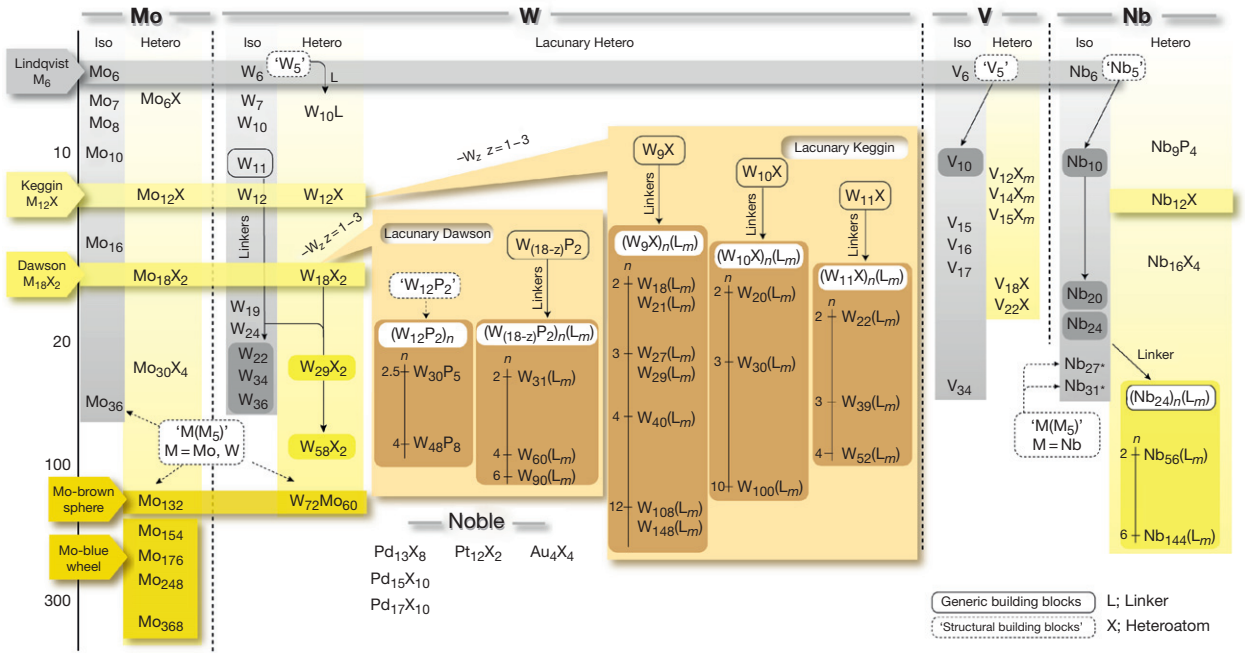

Figure 3 A POM periodic table using a classification based on building blocks.[12–15,18,21–29] The 'generic building blocks' shown as solid lines indicate they have been isolated as stable clusters: W_{11} isopolyanion, lacunary Keggin (W_9X, $W_{10}X$, $W_{11}X$), lacunary Dawson ($W_{(18-z)}P_2$), and Nb_{24} isopolyanions. These building blocks can be linked to form higher-nuclearity clusters of nuclearity *n*, by linkers L that contain a transition-metal ion, alkyl metals, or heteroions. For example, $(W_9X)_n(L_m)$ is composed of *n* W_9X building blocks assembled with several linkers of general formula L_m. Structural building blocks (in boxes with dashed lines) have not been isolated as clusters to date, but can be considered as building blocks for high-nuclearity POMs. These are: M_5 (one-metal lacunary Lindqvist; M = W, V, Nb), $W_{12}P_2$ (hexavacant lacunary Dawson), and $M(M_5)$ (pentagonal building blocks; M = Mo, W, and Nb). Note: solid and dashed arrows do not correspond to synthetic routes. In a separate category are the noble metal POMs, where X = As for the Pd compound, and X = S for the Pt compound.

POM clusters can be divided into three subsets depending on their structure, namely, heteropolyanions, isopolyanions, and Mo-blue and -brown, which are depicted in Figures 4 and 5:

(i) Heteropolyanions: These are metal-oxide clusters that include heteroanions such as SO_4^{2-} and PO_4^{3-}. These represent by far the most explored subset of POM clusters and much of this research has examined the catalytic properties of POMs with great emphasis on the Keggin $[XM_{12}O_{40}]^{n-}$ and the Wells–Dawson $[X_2M_{18}O_{62}]^{n-}$ (where M = W or Mo and X = a tetrahedral template) anions, which represent the archetypal systems (see Figure 4 for composition of the general POM structures). Tungsten-based POMs are robust and this fact has been exploited to develop Keggin and Dawson anions with vacancies, lacunary structures (most common are mono-, di-, and trivacant clusters) that can be linked using electrophiles to produce larger aggregates in a predictable manner. The development of lacunary POMs, based upon Keggin $\{M_{12-n}\}$ and Dawson $\{M_{18-n}\}$, tungsten-based POMs, is a large area and will not be explicitly covered here in detail.[24]

(ii) Isopolyanions: These are composed of a metal-oxide framework but without the internal heteroatom/heteroanion. As a result, they are often much more unstable than their heteropolyanion counterparts.[25] However, they also have interesting physical properties such as high charges and strongly basic oxygen surfaces, which means they are attractive units to use as building blocks.[26]

Author's personal copy

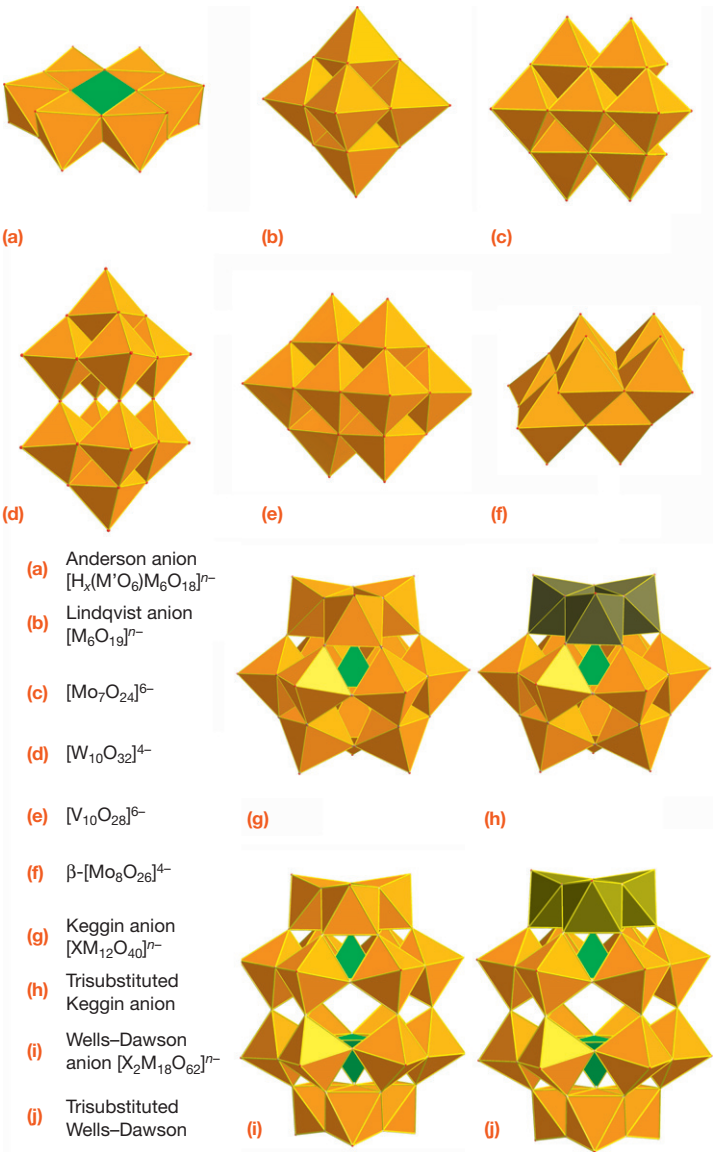

Figure 4 Representation of the most typical POM structures. Color scheme: The gold-colored $\{MO_6\}$ octahedra represent the addenda metal, M (Mo, W, V, etc.); the light green $\{MO_6\}$ represents the central heteroatoms; the dark green $\{MO_6\}$ represents the substituted addenda, often a $\{V\}_3$ cap; O, red.

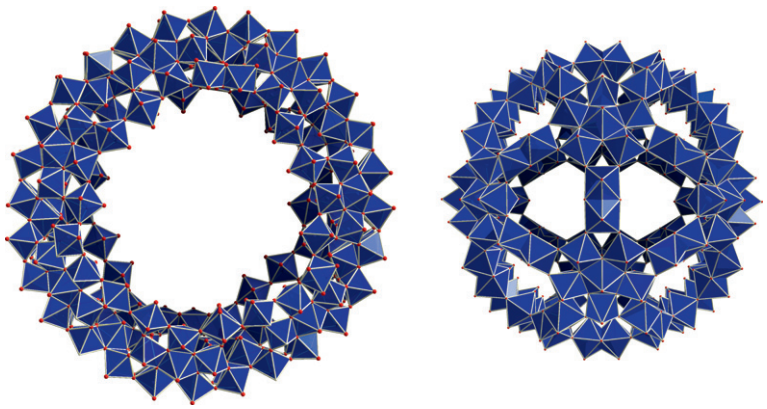

Figure 5 Polyhedra representation of the $\{Mo_{154}\}$ (left) and $\{Mo_{132}\}$ (right). Color scheme: Mo, blue (polyhedra); O, red.

Author's personal copy

(iii) Mo-blue and Mo-brown reduced POM clusters: These are related to molybdenum blue-type species, which were first reported by Scheele in 1783.[6] Their composition was largely unknown until Müller et al. reported the synthesis and structural characterization of a very high nuclearity cluster $\{Mo_{154}\}$ with a ring topology, crystallized from a solution of Mo-blue.[27] Changing the pH and increasing the amount of reducing agent along with incorporation of a ligand-like acetate facilitate the formation of a $\{Mo_{132}\}$ spherical ball-like cluster.[28] This class of highly reduced POM clusters represents one of the most exciting developments in POM chemistry with many potential spinoff applications in nanoscience which will be discussed later.

2.10.1.3 Synthesis and Assembly

POM clusters occupy a vast parameter space between the mononuclear metalate species and the bulk metal oxides, and the incorporation of heteroatom templates, heterometallic centers, lacunary building blocks, cations, and ligands all dramatically affect the overall architecture. The simple fact is that the architectural design principles are almost all empirically based, and an appreciation of the pH-dependent speciation of the metalates can often be the key starting point in any synthesis. Generally, the approaches used to produce POM-based clusters are simple, consisting of an acidic solution containing the relevant metal-oxide anions, molybdate and tungstate (vanadates tend to be synthesized at high pH).[14] POM systems are complex due to many thousands of combinatorially possible structure types, where each building block can itself adopt a range of potential isomers.

Synthetically, the route to produce new POM clusters is often very simple synthetic manipulations requiring a small number, or even just one step (so-called 'one-pot' synthesis), see Figure 6. The acidification, for example, of a solution of sodium molybdate will give rise to metal-oxide fragments, which increase in nuclearity as the pH of the solution decreases. This means that aqueous synthesis of POM clusters is the norm, and this can be carried out in the presence of simple metal cations; however, this can also be organic cations, and the solvent system can be extended to solvent mixtures, for example, water/CH_3CN. The synthetic variables of greatest importance in synthesizing such clusters are (1) concentration/type of metal-oxide anion, (2) pH, (3) ionic strength, (4) heteroatom type/concentration, (5) the presence of additional ligands, (6) reducing agent, and (7) temperature of reaction and processing (e.g., microwave, hydrothermal, and reflux).

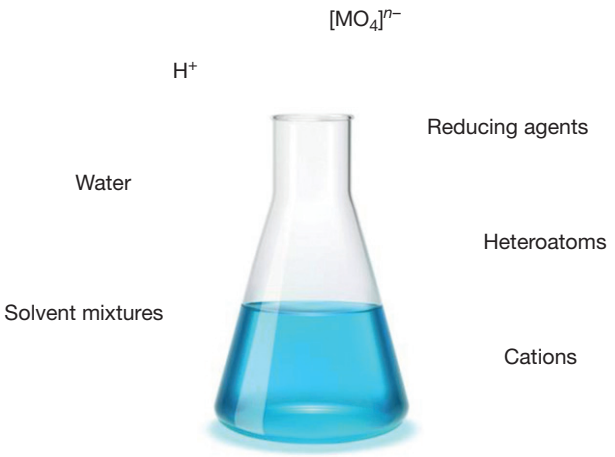

Figure 6 Representation of the multiparameter 'one-pot' methodology with most parameters listed that are often used in the synthesis/isolation of new POM clusters.

In particular, some recent developments in the synthesis of POMs can be used to search for new POM systems, like the use of protonated organic amine cations introducing an inverse cation templation effect,[25,30,31] or the application of mixed-solvent strategies, which can lead to the isolation of new clusters, for example, the sulfite-based polyoxomolybdate[32] and $[(P_2O_7)W_{17}O_{51}]^{4-}$.[33] Hydrothermal processing is another tool, becoming increasingly more popular and controllable, especially in the synthesis of POM-based coordination polymers.[34] Finally, the use of ionic liquids as solvent/cation directing species for the directed assembly of POMs is a new concept still in its early phase, but which holds great potential in the synthesis and development of functional POMs.[35,36]

2.10.2 Crystal Engineering by Cation Control

From a crystal engineering point of view, one important factor that affects the formation of a particular POM species, out of a vast library of candidates, relates to the crystallization process itself. This point is brought into sharp focus when one realizes that, although many reports focus on the POM framework exclusively, POMs are polyanions and cannot exist without the charge-balancing cations, which often define the network into which the anion is 'complexed.' In this way the cations themselves appear to be able to re-route or control the complex,[37] see Figure 7. Since the properties of the cations

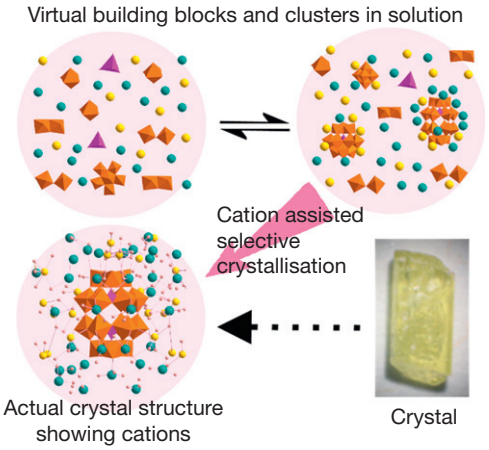

Figure 7 The formation of various structural archetypes in solution highlighting the role of cations in selective crystallization of a particular product. Yellow and green spheres represent different cations. The top left shows a range of 'virtual' geometrically possible units and the top right shows the cations complexing the clusters and pulling certain structures out of solution. The orange polyhedra represent the metal addenda, in this case W.

Author's personal copy

such as size, charge, symmetry, and solubility are found to modulate the reactivity of POM building blocks, the cations can affect the nature of the product obtained from a POM synthesis.[38–42] A proper match between the cations and anionic POM species is needed for effective crystallization; hence most often the product isolated in crystalline form may not necessarily be the one with the highest abundance in solution.[12] Figure 8 depicts the distribution of cations, anionic POM clusters, and their combined lattice arrangement in a true POM crystal structure, which highlights the vast number of counter-cations that are present in the structure.

As POM chemistry is now very well established after decades of research including intense underpinning structural studies, the initial structural and topological curiosity has been replaced by the quest for new tunable and functional clusters capable of exhibiting novel, and controllable physical properties.[14,26] This means that the crystal engineering of POM-based materials should be directed toward the incorporation of well-conceived functionalities into such systems in order to develop the materials aspects of POM chemistry. For example, POM synthesis, employing solution-processing methods, has great potential to allow the assembly of new solid-state materials using a molecular design approach.[25,43–52]

Using a crystal engineering-type approach toward predefined POM-based materials,[25] it can be argued that two things are most important – one, the discovery of novel POM building blocks and, second, to direct their self-assembly in a controlled way to form useful materials. To achieve these targets, a simple strategy can be applied, which is based on the use of bulky organic amine cations as counter-ions in POM synthesis.[25,43–52] The use of such bulky cations helps to isolate self-assembled POM species in one-pot reaction systems, thus preventing their rapid aggregation into clusters having stable uniform spherical topology. In addition, such cations together with other linker units are found to be capable of directing the self-assembly of POM building blocks into extended structures. Cronin et al. termed this approach as 'shrink wrapping,'[25,43–52] and mainly involves the use of organic amines such as hexamethylene tetramine (HMTA), triethanol amine (TEA), *N*, *N*-bis-(2-hydroxyethyl)-piperazine (BHEP), and morpholine, which are capable of acting as well-defined (encapsulating) cations, as well as ligands, buffers, and even as redox reagents in some cases, see Scheme 1. Further, it is possible to produce a number of discrete iso- and hetero-polyoxo clusters as well as many extended architectures using this simple, but efficient, concept.

2.10.3 Nonconventional and Chiral POMs

The majority of new structures reported for POMs every year is based on the traditional structures and metals, with only small variations and alterations. Over the last few years, the paradigm has started to shift, and a huge focus is now on designing new structures with built-in properties. Alongside this, there is a great interest in synthesizing new POM structures with novel metals, such as niobium, platinum, and palladium, functional groups, and properties, in the quest for innovative applications. Here some examples of novel and nonconventional POMs reported in the most recent years are presented.

2.10.3.1 Polyoxoniobates

The assembly of polyoxoniobates has mainly focused on isopolyniobates, for example, the $[Nb_6O_{19}]^{8-}$ Lindqvist ion. Nyman et al. reported the polyoxoniobate cluster type

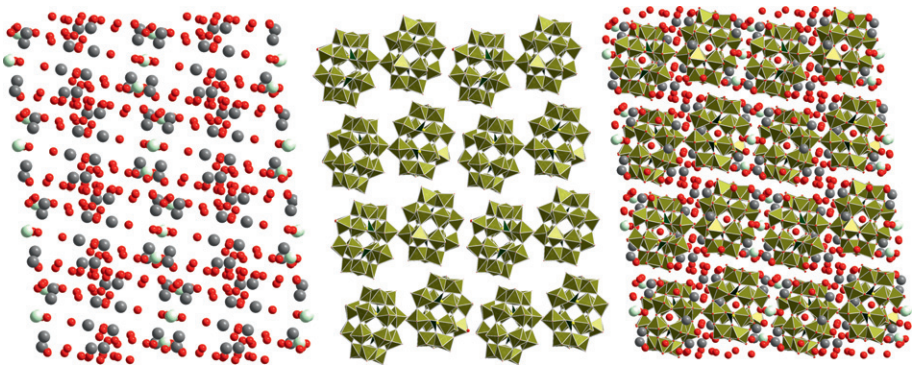

Figure 8 Packing diagrams depicting the separate and combined arrangements of cations and anionic POM clusters in a crystal lattice. Left: Only cations (pale green and gray spheres) and solvent water molecules (red spheres); middle: only POM clusters (yellow and green polyhedra) and; right: POM cluster anions, counter-cations and solvent water molecules together in a crystal lattice.

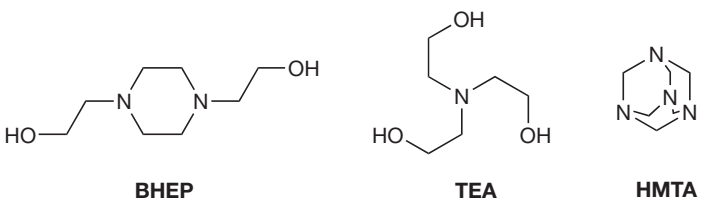

Scheme 1 Various shrink-wrapping cationic precursors used in studies reported by Cronin et al.[25,43–52]

Author's personal copy

$[Nb_{24}O_{72}H_9]^{15-}$.[53] The cluster can be derived from two fundamental structural types: the condensed octahedral $\{Nb_6\}$ ring and an open $\{Nb_6\}$-ring, which can serve as building blocks for even larger clusters and extended structures.[54] Cronin et al. have discovered two polyoxoniobates, $[HNb_{27}O_{76}]^{16-}$ and $[H_{10}Nb_{31}O_{93}(CO_3)]^{23-}$, which also incorporate pentagonal building units, and these clusters were assembled in the presence of a dibenzyldithiocarbamate, but the reason for their isolation is not yet known, see Figure 9.[55]

Further, Casey et al. reported the synthesis and characterization of a new type of POM structure $[Ti_{12}Nb_6O_{44}]^{10-}$,[56] which forms a super-octahedron. The 'super-Lindqvist' cluster has six Nb centers located on the vertices of the octahedron and 12 Ti atoms on the middle point of each of the 12 edges. The remarkable feature is that there is a central cavity large enough to hold another Nb atom, but it is empty in this particular case. In addition, it may be possible to embed these clusters in titania and other oxides to produce novel materials based upon the Nb oxides. It will be interesting to see if a range of new structures will emerge by adopting new processing approaches, and if new physical properties, for the normally inert Nb center, can be found and exploited, especially given the new pentagonal structure architectures discovered and described above.[53] Polyoxoniobates are found to have an opposite solubility trend in water (Cs salt most soluble, Li salt least soluble) compared to what is expected from the classical aqueous solubility behavior of POMs, as first discovered with the $[Nb_6O_{19}]^{8-}$. This was also confirmed to be true for larger niobium POM structures. This might open up the possibility to investigate further chemistry and applications of heteropolyniobates, including ion association in solution, incorporation into functional surfaces and materials, homogeneous catalysis, and microbiological applications.[57,58]

2.10.3.2 Uranium

Although the classification of POM clusters can be very helpful (Figure 3), the central paradigms are constantly being challenged as a result of new synthetic and structural developments. For instance, the peroxide-uranium compounds are certainly not classical POM clusters, but exhibit certain key similarities, especially to the larger structures.[59] The peroxide groups bridging between uranyl ions cause the U–(O_2)–U unit to be bent. This bent configuration favors formation of cage clusters, rather than sheets of uranyl polyhedra, and a rapid self-assembly of uranyl polyhedra into crown clusters was reported by Sigmon.[60]

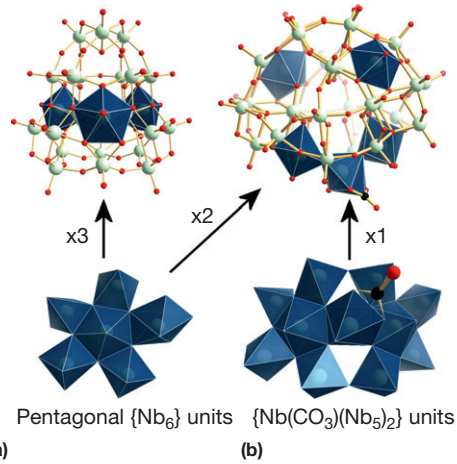

Figure 9 Structure of (a) $[HNb_{27}O_{76}]^{16-}$ and (b) $[H_{10}Nb_{31}O_{93}(CO_3)]^{23-}$. The bottom figures represent the pentagonal $\{Nb_6\}$ unit and the carbonate incorporating $\{Nb(CO_3)(Nb_5)_2\}$ unit. Color scheme: Nb, pale green (spheres) and cerulean blue (polyhedra); O, red.

2.10.3.3 Palladium

Examples of molecular palladium oxide clusters that have emerged first by Kortz et al.[61] who demonstrated the possibility of expanding the family of POMs to palladium. Until now $\{Pd_{13}\}$,[61] $\{Pd_{15}\}$,[62–64] and a $\{Pd_{15}\}$cluster host encapsulating a $\{Pd_2\}$ dinuclear guest,[62] $\{Pd_7V_6\}$,[65] and $\{Cu_2Pd_{22}\}$[66] have been reported. The palladium(II) ions retain a square-planar geometry that is normally seen for Pd(II), in contrast to those of octahedral environments in all other typical POMs. Interestingly, although the Pd(II) centers do not support Pd=O moieties in these complexes, these clusters can be at least compared with POM-based structure types and further developments in this field, for example, replacement of the AsO_4^{3-} groups, or even substitution of the Pd for other metals, will lead to a large variety of new structures. Although this has gained a lot of attention, due to the potential for new developments, it should be noted that Wickleder et al. presented a $[Pt_{12}O_8(SO_4)_{12}]^{4-}$ in 2004, which has been rarely cited.[67] More recently, Kortz et al. successfully synthesized an oxometalate using gold, the polyoxoaurate $[Au^{III}{}_4As^{V}{}_4O_{20}]^{8-}$.[68] The $\{Pd_{15}\}$ cluster host encapsulating a $\{Pd_2\}$ dinuclear guest[62] is presented in Figure 10.

From observations by Hill et al., it was suggested that POM clusters can act as strong pi-acceptor ligands to stabilize late-transition-metal oxo groups, thus allowing the isolation of the first oxo complexes of the noble metals Pt, Pd, and Au. Among them the Pt(IV) complex $[O=Pt(H_2O)L_2]^{16-}$ (L=$[PW_9O_{34}]^{9-}$) received special attention, not only because this compound represented a breakthrough in the field of late transition metals, but also because oxoplatinum intermediates are believed to be key participants in many oxidative processes occurring on platinum surfaces.[69] This compound is interesting as it challenges the concept of an oxo-wall,[70] and also raises real issues about the nature of the bonded configuration of the terminal platinum-oxo bond (oxo or hydroxide),[69] which has been the subject for discussion.[71,72] This is also relevant for the related palladium[73] and gold compounds.[74] However, in a very recent development Hill published a correction to the oxo-wall papers[75] giving a new interpretation of the data indicating that the metal in the [M=O] moiety had been erroneously assigned in each of the cases to either Pt, Pd, or Au, indicating that the principle of the oxo wall is still valid.

2.10.3.4 Peroxide Ligands

Moving from oxo-based systems, new types of POM systems are also being presented that incorporate peroxide-type ligands. For instance, Neumann et al. have reported the isolation and characterization of a peroxide 'end-on' $\{Fe^{III}–O_2\}$ POM-based compound in water with unusual properties.[76] The

Author's personal copy

compound is stabilized by hydrogen bonding and is derived from a reaction between a multi-iron(II) POM and H_2O_2. The structure contains a coordinated peroxide unit with an almost linear Fe–O–O bond angle which has been characterized by x-ray diffraction and electron energy-loss spectroscopy.[76] Conventionally, the peroxide ligand adopts a side-on, bridging coordination motif as found in the $[(UO_2)]_{60}$ structure and also in the 6-peroxo-6-zirconium crown $[M_6(O_2)_6(OH)_6(\gamma\text{-}SiW_{10}O_{36})_3]_{18}$ (M = Zr, Hf); see **Figure 11**.[59,77] These systems are interesting since the use of highly charged 'POM ligands' to stabilize reactive oxo, peroxo, or superoxides is very important for the development of new catalysts, mechanistic insight, and structural motifs.[78]

2.10.3.5 Chirality

The wide application of POMs, including catalysis, biology, medicine, magnetism, material science, and photochemistry, means that there is considerable scope for the development of truly chiral metal-oxide architectures. Historically, chiral POM clusters can be formed via structural vacancies and geometrical distortions. However, such enantiomers are very easily racemized and are very difficult to separate and isolate. One strategy that may overcome these limitations would be to 'graft' chiral organic ligands directly onto the POM framework.[79] Also, the use of heterometal ion linkers can be used to link chiral POM fragments. Chiral frameworks can be produced from the linkage of achiral units, for example, by producing a twist between the linked POM anions, or the metal cation sandwiched between the two anions coordinates in a distorted square-antiprismatic geometry.[80] Since the sandwich framework produced by linking chiral POM building blocks can be either homochiral or heterochiral (meso), heterometal cations can mediate between the POM anions and the organic molecules. For instance, Zr(IV) has been used to link a chiral tartrate and two achiral lacunary Wells–Dawson POM units, $\alpha\text{-}[P_2W_{15}O_{56}]^{12-}$, see **Figure 12**.[81] High-dimensional chiral frameworks have been built by the incorporation of suitable achiral organic molecules, metal cations, and POM building units even without any chiral auxiliaries. In addition, it is conceptually feasible to use complexes such as $[Co(en)_2]^{3+}$, to partially substitute some Mo or W atoms in POM structures, leading to chiral motifs embedded in the clusters by replacing one of the 'bis' chelating ligands with the POM fragment itself.

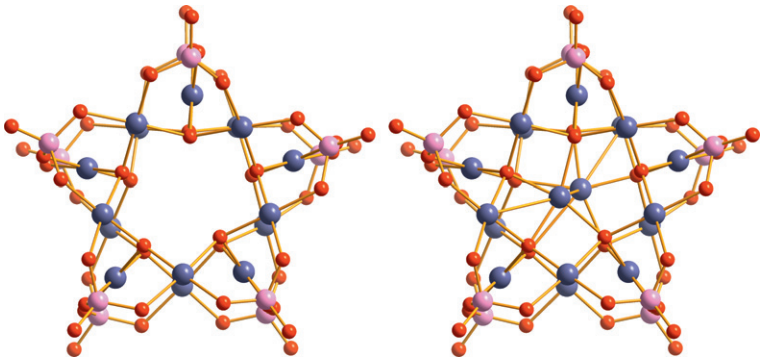

Figure 10 Illustration of different structures between $\{Pd_{15}\}$ (left) and $\{Pd_2 \subset Pd_{15}\}$ (right). Color scheme: Pd, dark purple; P, pink; O, red.

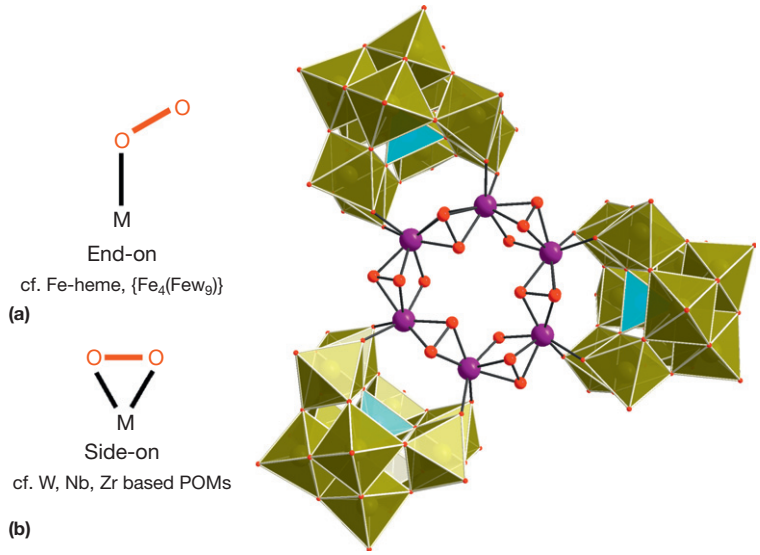

Figure 11 End-on (a) and side-on (b) coordination of the peroxide ligands. Structure of 6-peroxo-6-zirconium crown $[Zr_6(O_2)_6(OH)_6(\gamma\text{-}SiW_{10}O_{36})_3]^{18-}$. Color scheme: W, green (polyhedra); Si, light blue (polyhedra); O, red.

Author's personal copy

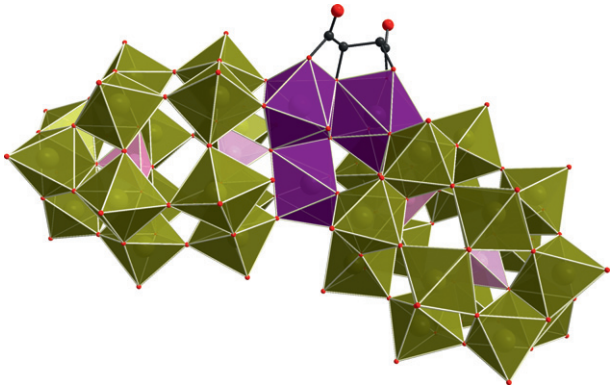

Figure 12 The structure of $[\alpha\text{-}P_2W_{15}O_{55}(H_2O)]Zr_3(\mu_3\text{-}O)(H_2O)(L\text{-tartH})[\alpha\text{-}P_2W_{16}O_{59}]^{15-}$. Color scheme: W, green (polyhedra); P, pink (polyhedra); Zr, purple (polyhedra); O, red; C, black.

Indeed, the exploitation of the charge on POMs by using chiral cations could be very important to produce functional hybrids. A novel type of noncovalently immobilized POM catalysts, where the POM is $\{PW_{12}O_{40}\}$, using magnetic nanoparticles as supports was reported by Cheng et al.,[82] resulting in reusable acid catalysts and catalyst supports for chiral amines. For an extensive overview of chiral POMs, see the reference by Thorimbert et al.[83] and references therein.

The key limitation in the synthesis of chiral POMs is that the enantiomers are easily interconverted and/or difficult to isolate, and a common approach toward obtaining chiral resolution is by employing chiral cations or fractioned crystallization. Statistically, between 5% and 10% of all racemized conglomerate crystals can be resolved spontaneously upon crystallization, and some chiral POMs can be formed using spontaneous resolution.[17,84–86] This area will certainly develop further with the key goal to form chiral POM–metal frameworks that are well defined, stable, and can be both detected and exploited, for example, chiral catalysis, sensing, or electronically active systems. One novel aspect may be to 'imprint' the chiral features in the cluster by self-assembling the cluster using structure directing chiral cations. This approach extends the 'shrink-wrapping' idea first presented by Cronin et al. to allow more intrinsically and structurally complex POM clusters to be assembled.[25]

2.10.3.6 Oxothiometalates

Oxothiometalates constitute a subclass of the POM family which consists of considerably fewer members than traditional POMs. The polyoxothiometalates (POTMs) bear little resemblance to their oxo-based analogues due to the fact that the sulfide ion is larger than the oxide, hence is a poorer pπ donor, and easier to oxidize.[87–89] Most reported POTM compounds are structurally based on conventional architectures of low nuclearity, ranging from the mononuclear anion, $[MoO_{4-n}S_n]^{2-}$ to tetranuclear oxothiomolybdate clusters. Cronin et al. reported a direct preparation method of the nanosized oxothiometalate $\{Mo_{40}\}$ wheel, $[(Mo_8O_{28})_4(Mo_2O_2S_2)_4]^{24-}$, previously described by Cadot et al.[90] Cronin employed the discrete $\{Mo_2O_2S_2\}^{2+}$ oxothio cation as the inorganic linker in the presence of a molybdenum source to give the desired product in considerably improved yield for such a large architecture. The aforementioned synthetic method simplifies the formation of the $\{Mo_{40}\}$ wheel in one single step under mild conditions (room temperature) obtaining good yields, which makes it energetically more favorable and less time consuming. Furthermore, high-resolution electrospray ionization-mass spectrometry (ESI-MS) studies on the reaction mixtures revealed the formation and demonstrated the structural integrity of the fundamental synthon, $\{Mo_8O_{28}\}$, in solution. The direct observation of the nanosized architectures in aqueous media is of great importance. It provides additional information regarding the available library of building units in solution while also unveiling crucial information to help postulate testable hypotheses with regard to the formation mechanism of such complicated chemical systems. Finally, the observation of the unprecedented $\{Mo_8\}$ species in solution is very important as it demonstrates its relevant stability under the experimental conditions and this opens the door for further exploration and design of new materials with potentially intriguing properties.[89]

2.10.4 Mo-Blue and Mo-Brown

Since the discovery of the $\{Mo_{154}\}$ 'big-wheel'[27,91] and the $\{Mo_{132}\}$ 'big ball' or Keplerate[28,92] clusters by Müller et al., this area of chemistry has continued to inspire chemists to both understand and utilize the unique building blocks[93] present in these materials.[94] Much progress has been made in both the wheel and ball systems including sizing of the clusters,[95] removal of inner building block fragments, addition of ligands, electrophiles, and even promoting growth processes.[24,92] The formula for the $\{Mo_{132}\}$ is $[Mo^{VI}{}_{72}Mo^{V}{}_{60}O_{372}(MeCO_2)_{30}(H_2O)_{72}]^{42-}$, and is made up of 12 $\{(Mo^{VI})Mo^{VI}{}_5\}$ pentagons and 30 $\{Mo^{V}{}_2\}$ dumbbells. The pentagonal component consists of a central $\{MoO_7\}$ unit edge sharing with five $\{MoO_6\}$ octahedra. Each $\{Mo^{V}{}_2\}$ unit links two $\{MoO_6\}$ octahedra in different pentagonal units. However, the 30 $\{Mo^{V}{}_2\}$ units can be replaced with, for example, Fe^{III}, Cr^{III}, V^{IV}, and Ln^{III}, resulting in $\{Fe_{30}Mo_{72}\}$,[95] $\{Cr_{30}Mo_{72}\}$,[96] $\{V_{30}Mo_{72}\}$[97]as well as $\{Ln_6Fe_{24}Mo_{72}\}$.[98] Following the same overall $\{M_{102}\}$ theory, a $\{Mo_{30}Mo_{72}\}$ has also been reported by Müller et al.[99] The giant wheels represent nanosensors and nanoreactors, enabling the initiation of chemical processes at different positions, like a 'structured landscape,' and can even be used as robust synthons for the construction of compounds with typical solid-state structures, a situation comparable to crystal engineering.[91] The potential functionality of these clusters and the use of the spherical systems as functional nanospaces and models for molecular uptake and storage and as artificial cell models are discussed in Section 2.10.10.

The reduction of molybdate in the presence of Eu(III) ions at pH 1–2 with ~20% of the added molybdate reduced to Mo(V) leads to a giant wheel-shaped cluster, similar to the archetypal $\{Mo_{154}\} = [Mo_{154}O_{462}H_{14}(H_2O)_{70}]^{14-}$ but this time the inclusion of the Eu(III) ions leads to the assembly of a giant elliptical cluster dimer $\{Mo_{256}Eu_8\} = [\{Mo_{128}Eu_4O_{388}H_{10}(H_2O)_{81}\}_2]^{20-}$ with a diameter of ca. 4 nm, see Figure 13. It appears that the inclusion of the Eu(III) ions causes a dramatic increase in curvature, when compared to the original $\{Mo_{154}\}$ wheel, which results in the elliptical shape of the new cluster.

Author's personal copy

In a further dramatic development a new $\{Mo_{368}\}$ 'lemon'-shaped cluster was synthesized with the approximate formula $[H_{16}Mo_{368}O_{1032}(H_2O)_{240}(SO_4)_{48}]^{48-}$.[100] This cluster was synthesized from a solution acidified with sulfuric acid and this allowed the incorporation of the sulfate anion within the cluster framework that significantly alters the cluster framework compared to the wheel-type clusters which are synthesized under similar conditions.[101] The lemon-shaped cluster was synthesized at low pH (1–3) and with 30% of the available molybdate reduced to Mo(V). Thus, the 'lemon' cluster is more highly reduced than most 'Mo-blue' species isolated to date and includes 48 sulfate anions on the inner sphere of the cluster. The cluster incorporates both positively and negatively curved surfaces and has a maximum diameter of ~5 nm, see Figure 14.[102]

While Müller et al. focus on 'one-pot' reactions, Cronin et al. were able to maintain an off-equilibrium reaction system where the degree of reduction of the polyoxomolybdate clusters was carefully controlled. To achieve this reaction state, screening of the synthetic parameters – for example, the concentration of molybdate, reducing agent, pH, and ionic strength – was required to determine the correct flow rate. After optimizing the flow system, it was possible to isolate and trap, by crystallization, a key intermediate in the assembly of a wheel-type molybdenum blue nanocluster, whereby single crystals were formed in the flow reactor and isolated by halting the flow and filtering the product after a given run time of 2–3 days. Specifically, a hollow $\{Mo_{150}\}$ wheel that hosts a $\{Mo_{36}\}$ cluster that is bound to the central cavity of the ring species by charge-balancing sodium cations was characterized, and in the solid state the wheel itself is weakly covalently linked through five oxo-bridges into chains. This host–guest complex shows features indicative of an intermediate electronic and structural state, and Cronin et al. postulate that the $\{Mo_{36}\}$ cluster acts as the key template in the formation of the molybdenum blue ring, see Figure 15.

2.10.5 Analytical Tools

As a natural consequence from the tremendous interest in POMs, the analytical techniques and approaches are improving and forever expanding alongside the new research. Cryospray ionization (CSI) and ESI-MS have become great tools for POM scientists in the characterization of new compounds and compound mixtures. However, these types of mass spectrometry techniques do have certain limitations; in particular, it is not possible to separate compounds with the same mass/charge ratio. Ion mobility spectrometry-mass spectrometry (IMS-MS) has been used to overcome this challenge in protein research, and Cronin et al. applied the same technique to POM compounds.[103] The technique successfully separates overlapping envelope peaks depending on the cross section of the various species. More information about spectroscopy of inorganic compounds can be found in Chapter 9.16 of this series.

2.10.5.1 Mass Spectrometry

2.10.5.1.1 ESI-MS and CSI-MS

It is a great challenge to understand the underlying self-assembly in the formation of POMs. A successful approach to

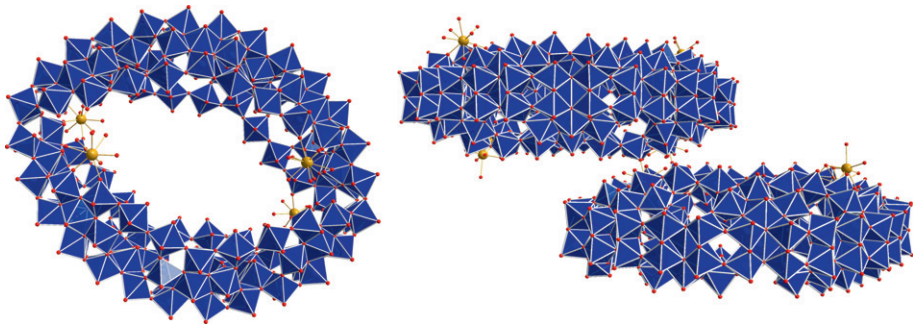

Figure 13 The structure of the elliptical $\{Mo_{128}Eu_4\}$ wheel and the structure of the full dimeric $\{Mo_{256}Eu_8\}$ cluster unit. Color scheme: Mo, blue (polyhedra); Eu, gold; O, red.

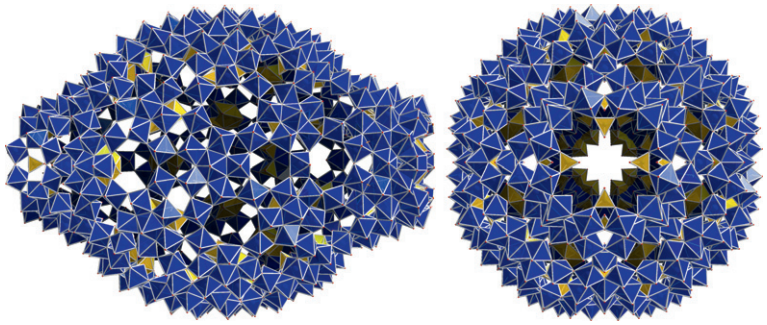

Figure 14 The structure of the blue $\{Mo_{368}\}$ 'lemon' cluster, shown side- and end-on. Color scheme: Mo, blue (polyhedra); S, yellow (polyhedra); O, red.

Author's personal copy

investigate the self-assembly processes and nature of POM clusters is utilizing high-resolution time-of-flight (TOF)-MS (both ESI and CSI) to examine the structures and the assembly/disassembly of high-nuclearity POMs and coordination clusters.[14] POMs are ideal candidates for MS studies as they have complex isotopic envelopes resulting from the high number of stable isotopes of tungsten and molybdenum, and they are intrinsically charged. This allows complete determination of the cluster formula down to the last proton by matching the calculated versus experimentally obtained envelopes. MS studies of unknown POM systems have enormous potential to aid the discovery processes as well as allow studies to unravel the complex self-assembly mechanisms.[17]

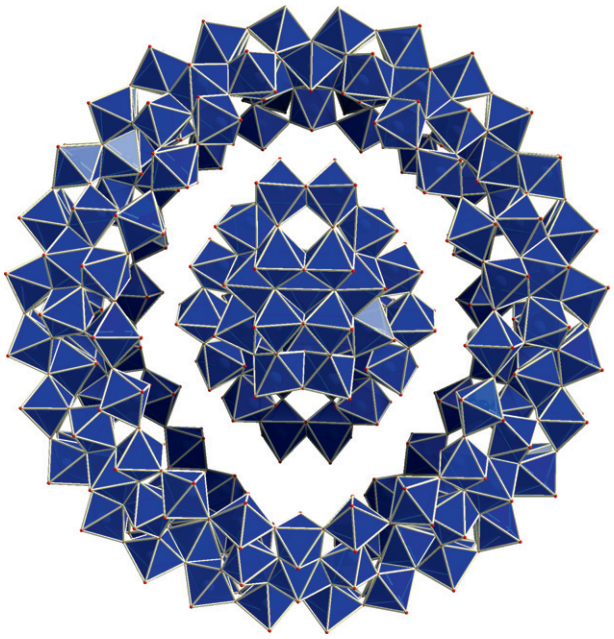

Figure 15 A polyhedral representation of the nanoscale $\{Mo_{36}\}\subset\{Mo_{150}\}$ wheel. Sodium cations have been omitted for clarity, although there are ~22 positions on the inner side of the ring where sodium resides, of which 12 directly bridge the template to the outer ring. The host and the guest are also connected by a series of hydrogen bonds. Color scheme: Mo, blue (polyhedra); O, red.

ESI-MS has recently been used extensively to investigate many types of POMs including vanadates, niobates, tantalates, chromates, molybdates, tungstates, and rhenates.[17,104] Further, MS can be used to probe mixed-metal clusters, authenticate the cluster composition of $\{Mo_{17}V_3\}$,[105] $\{W_{19}\}$,[106] $\{W_{181}\}$,[107] etc., probe protonation versus heteroatom inclusion,[104] identify new isopolyoxotungstates and functionalized POMs in solution,[108] explore the formation of POM-based nanostructures,[109] and to investigate the mechanism of POM self-assembly.[110,111] Also, MS studies can help in the synthesis of complex hybrid architectures, for example, for the asymmetric Mn-Anderson POM cluster, $[N(C_4H_9)_4]_3[MnMo_6O_{18}(C_4H_6O_3NO_2)(C_4H_6O_3NH_2)]$, which is very similar to its symmetrical counterparts when it is a di-NO_2 or di-NH_2 cluster. MS is useful in this case to establish separation protocols for complex structure frameworks that may be synthetic intermediates, as well as fragmentation studies that look at the stability of the clusters, see **Figure 16** for a general example.[112,113] More recently, Ma et al. studied the fragmentation in gas phase of a series of POM clusters. Together with common species from protonation, alkali metal association, and loss of water, the fragmented species $[W_xO_{3x+1}]^{2-}$ and $[PW_{12-x}O_{39-3x}]^-$ $(x=6–9)$ were observed. These results highlight the importance of ESI-MS in the characterization of complex POM anion clusters[114] along with the investigations of the reaction mechanism of polyoxoniobates with hydrogen peroxide using ESI-MS.[115]

CSI-MS is of interest for investigations of labile POM systems because standard ESI-MS studies of such systems have been limited by the use of high temperatures utilized in the ionization process. The use of low-temperature gases promotes ionization of the target molecules, not by desolvation, but by increasing the polarizability of the target molecules at low temperature (i.e., the result of higher dielectric constant at low temperature).[116] This allows the molecular ions of unstable species to be generated and transferred efficiently into the MS detector with minimal fragmentation effects.[17] In recent work, Cronin et al. have employed CSI-MS to investigate unstable POM complexes,[110] and to examine reaction mechanisms.[111] Using CSI-MS it is possible to screen new cluster systems, as reported by Cronin et al. where it was used to establish if tellurium could be embedded as a heteroanion into a Dawson-like cluster cage, as well as to monitor the *in situ* reduction of Te^{VI}

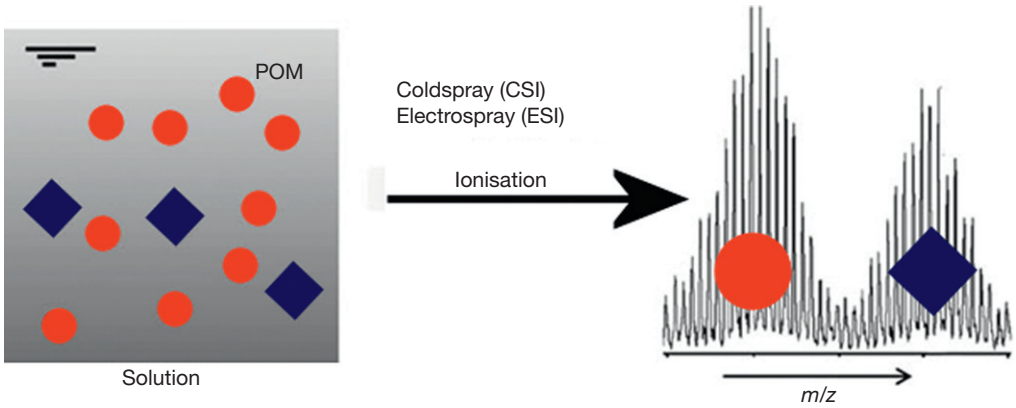

Figure 16 ESI and CSI mass spectrometry in the investigation of complex isotopic systems, such as POM-based molecules.

Author's personal copy

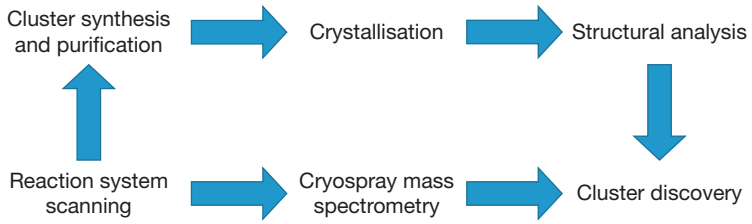

Scheme 2 The three steps for conventional cluster discovery compared to the one-step approach using cryospray mass spectrometry.

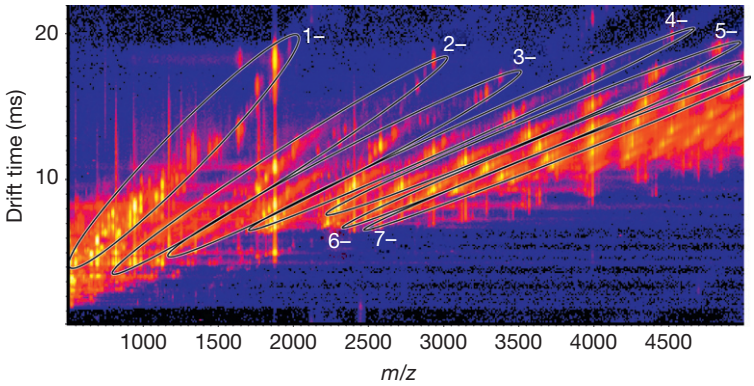

Figure 17 An example of a 2D IMS-MS spectrum. The diagonal lines of similarly charged species are encircled by ellipsoids and the charges of these species are given in white.

to Te^{IV}.[117] This represents a new approach to the discovery of nanoclusters, utilizing CSI-MS to directly probe the reaction solution, allowing the discovery of new guests inside cage-like nanocluster architectures, see Scheme 2.

2.10.5.1.2 IMS-MS

POM building units are variable in terms of not only size and charge[109] but also shape and conformation.[118] Conventional MS allows for the separation of the anionic clusters by their mass and charge, that is, their m/z ratio, but the supramolecular quaternary structure, or isomers with the same size and charge, cannot be resolved by this method.[112] Cronin et al. described the use of IMS-MS, previously used to examine protein structure and dynamics as well as some preliminary studies on coordination compounds,[119–121] as a new tool to probe metal-oxide systems, allowing size separation and investigation of supramolecular assemblies as well as the conformation or folding of the cluster architectures. The Anderson clusters were chosen as model compounds for the primary investigative studies since they are a well-characterized class of compounds.[111–113] Also, the organic derivatives of these clusters represent a well-defined library allowing the physical or chemical properties of the hybrid to be influenced by choice of the tethered organic group.[122,123] The IMS-MS studies were performed on an ion-mobility mass spectrometer that combines traveling wave IMS (TWIMS) with quadrupole/time-of-flight (Q/ToF) MS.

MS experiments of Mn-Anderson compounds without the use of ion-mobility separation tend to show complex overlapping envelopes of species. This indicates the presence of supramolecular assemblies, possessing different charge states but the same m/z ratio. To deconvolute these envelopes, IMS was performed for the size separation of the polymolecular aggregations, allowing for the assignment of their overall composition. Figure 17 shows a two-dimensional (2D) IMS-MS spectrum of the Mn-Anderson compound $[(TBA)_2[MnMo_6O_{18}((OCH_2)_3C\text{-}NH\text{-}C_9H_9)_2]]^{1-}$ where the x-axis shows the m/z range and the y axis shows the drift time; the peak intensity is displayed according to a color code on a logarithmic scale. The various high-intensity peaks along a certain m/z value represent the individual envelopes (species) which would be overlapping at that exact m/z value in a spectrum obtained from a conventional MS experiment.

Photoresponsive ligands containing azo bonds, which can be changed from *trans* to *cis*, in conjunction with the Mn-Anderson cluster, were also examined by IMS-MS, and the conformational change from *trans* to *cis* was successfully observed. Although the link between solution chemistry and gas phase has yet to be established, the strong ligand interactions indicated by the supramolecular assemblies found in the IMS-MS measurements give strong indications for future studies in surface chemistry[112] and vesicle formation.[124,125] IMS-MS opens up a crucial new dimension allowing the characterization of clusters according to both their size and charge, and therefore their charge density, as well as investigating the supramolecular chemistry and structures of the clusters in the gas phase.

2.10.5.2 Electrophoresis

Gel electrophoresis, a tool for separating compounds depending on mass and charge, has also been proven useful in the characterization and separation of POMs.[126,127] Cronin et al.

Author's personal copy

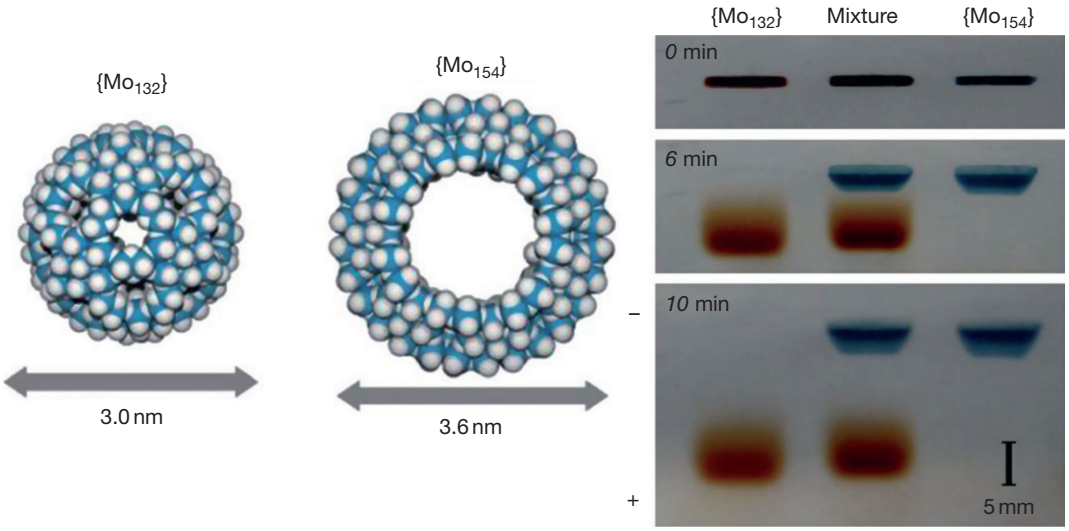

Figure 18 Space-filling models, where the blue and white spheres correspond to the metal (M = Mo or W) and oxygen ligands, respectively. The chemical formulas of the {Mo_{132}} and {Mo_{154}} complexes are $(NH_4)_{42}[Mo_{132}O_{372}(CH_3CO_2)_{30}(H_2O)_{72}]\cdot\sim 300H_2O\cdot\sim 10CH_3COONH_4$ and $Na_{15}[Mo_{154}O_{462}H_{14}(H_2O)_{70}]_{0.5}[Mo_{152}O_{457}H_{14}(H_2O)_{68}]_{0.5}\cdot\sim 400H_2O$, respectively.

proved that the two compounds 'molybdenum blue' {Mo_{154}} and 'molybdenum brown' {Mo_{132}} moved toward the same anode with different mobilities, but that the {Mo_{132}} sphere moves faster than the {Mo_{154}} wheel, see **Figure 18**. The higher mobility of the {Mo_{132}} ball can be rationalized when one considers its smaller size and higher charge than the {Mo_{154}} wheel.[128] The ability to use gel electrophoresis to measure mobility and hence characterize the surface charge density of nanoscale POM clusters represents a major breakthrough and opens up new possibilities to explore a large variety of other nanoscale clusters, nanoscale particles, and nanoscale-molecular aggregates, for example, metal–organic frameworks (MOFs) or any other large nanoscale structures of high charge and large size.

2.10.5.3 Surface Analysis

Surface-related techniques have shown great potential in the analysis of POMs in the quest for POM-based devices. Langmuir–Blodgett (LB) depositions have been extensively utilized on POMs, with several interesting results.[122] Cronin et al. deposited POM–organic hybrids onto solid substrates via the LB technique, and sequentially analyzed the patterns with atomic force microscopy (AFM), scanning capacitance microscopy (SCM), and scanning capacitance measurements.[112,129] However, when similar compounds are deposited onto solid substrates by drop casting rather than the LB technique, no defined, individual patterns were obtained.[130] The growing number of investigations into POM clusters on solid substrates reported has been made possible not only due to the large amount of novel POM clusters available, but also because of the developments of high-quality and sophisticated analytical surface tools. Scanning probe microscopy (SPM) is a broad term for all types of probe microscopy, and it includes AFM,[112,129,130] also known as scanning force microscopy (SFM). Also available are high-quality SCM,[129] scanning electron microscopy (SEM),[131] transmission electron microscopy (TEM),[131] and scanning tunneling microscopy (STM).[132] Other techniques such as surface-enhanced Raman scattering (SERS) and scanning near-field optical microscopy (SNOM) are cutting-edge techniques with enormous potential in the analysis of POM structures on surfaces and applications.

2.10.6 POM–Organic Hybrids

Given the exceptional physical and structural properties intrinsic to POM superstructures, the ability to covalently modify the metal-oxide cage in a reliable and predefined manner holds exceptional promise for the development of molecular materials that bridge the gap between molecular organics and bulk semiconducting oxides (see **Chapter 2.14** for a discussion on hybrid semiconductor materials). POM–organic hybrid structures are often divided into two classes.[122,123] The first (class I) is noncovalently bound organic species, usually via electrostatic interactions, hydrogen bonding, etc., and the second (class II) is those structures which contain an organic component covalently bonded to the POM framework, usually via strong covalent or iono-covalent bonds. Class I POM–organic hybrids can easily be obtained by employing organic cations, which can drastically alter the properties of the original POM cluster.[131,133]

For class II hybrids, the organic ligand can substitute an oxo group in the POM framework, and be directly linked to one or more of the metallic centers. The nucleophilic character of the oxygen atoms localized on the surface of POMs can also lead to covalent interactions with electrophilic groups bearing organic moieties.[122] The linking can occur via p-, d-, and f-block metals, and is a rapidly evolving field that can combine the best properties of the transition-metal-based POMs and functional organic molecules[134] (e.g., fully conjugated organic moieties) and stabilize otherwise unstable architectures.[135] Here the focus is on reported examples where the organic ligands have substituted an oxo group in the POM framework with either an imido or an alkoxy functional group, see **Figure 19**.

Author's personal copy

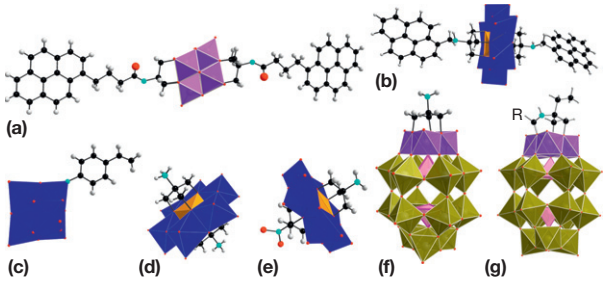

Figure 19 (a) Pyrene-alkoxy functionalization of the $\{V_6\}$ Lindqvist,[136] (b) pyrene-alkoxy functionalization of the Mn-Anderson,[137] (c) imido-functionalized $\{Mo_6\}$ Lindqvist,[138] (d) TRIS-functionalized Mn-Anderson,[139] (e) TRIS–NH_2 and –NO_2 asymmetrically functionalizsed Mn-Anderson,[113] (f) TRIS-functionalized $\{P_2W_{15}V_3\}$ Wells–Dawson,[109] and in (g) the amine-functionaliszd $\{P_2W_{15}V_3\}$ Wells–Dawson.[140,141] Color scheme: W, green (polyhedra); Mo, blue (polyhedra); V, purple (polyhedra); Mn, orange (polyhedra); O, red; N, cyan; C, black, H, white.

The functionalization of the Lindqvist anion is well documented and the $\{Mo_6\}$ cluster can be functionalized by replacing Mo=O groups with Mo=N–R moieties,[138,142] and the bridging oxo groups can be replaced by amine groups.[143] In 1983 tris alkoxide ligands were found to link POMs,[144] and in 1990 examples of alkoxide ligands linked to polyoxovanadates were obtained.[145] Müller et al. expanded this field with tris alkoxide moieties grafted onto phosphorus-containing heteropolyoxovanadates.[146] The great potential for the alkoxide linkage between the organic and inorganic moieties lies in the direct incorporation of the alkoxide oxygen atoms into the actual metal-oxide framework.[139,146,147]

The first examples of TRIS ((tris-hydroxylmethyl)aminomethane)-functionalized Mn-Anderson clusters were reported by Hasenknopf et al.[139] The ligation of Anderson clusters with tris alkoxy ligands onto both sides of the cluster can be used to add large organic aromatic groups, for example, pyrene, symmetrically and unsymmetrically on two sides of the Mn-Anderson cluster.[113,137]. There is still a growing interest in the functionalization of the Anderson cluster as well as varying the central heteroatom, variations in the organic ligands and how they are attached to the metal-oxide core, along with variations in the cations employed. Wei et al. reported a single-side organically functionalized Anderson-type POM,[148] presenting a new approach toward asymmetrically functionalized Anderson structures, offering great potential in the synthesis of new POM–organic hybrids.

Wang et al. reported a combination of two organo-imido functionalized $\{Mo_6\}$ Lindqvist clusters and a TRIS Anderson cluster, where the free amine group in the TRIS moiety is used to functionalize the $\{Mo_6\}$ units. The obtained nanoscale POM–organic hybrid molecular rods that assembled from two types of POMs through strong covalent linkages with a bifunctional organic ligand is chiral[149] (**Figure 20**).

The ligation of $\{V_6\}$ Lindqvist anions functionalized with organic ligands via tris-alkoxy linkers has also been reported, with two recent examples presented by Hill and Liu et al.,[136] and Wei et al.[150] In the case reported by Hill and Liu the functionalization is both symmetrical and asymmetrical, resulting in fluorescent vesicles under the right conditions.

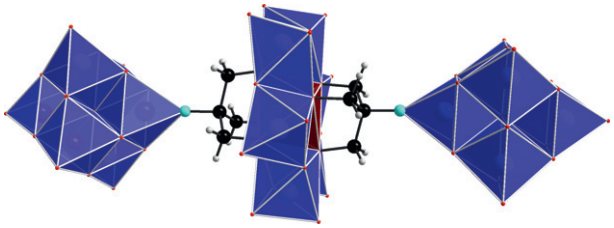

Figure 20 A polyhedra presentation of the joint Anderson–Lindqvist structure. Color scheme: Mo, blue (polyhedra); Fe, brown (polyhedra); O, red; N, cyan; C, black. The equivalent structure was also obtained with Mn (III) as the central heteroatom.

Wei et al. reported symmetrically substituted $\{V_6\}$ clusters with two long-chain ligands using an esterification, presenting a new route to more conveniently and economically functionalized polyoxovanadates.

The Dawson-type cluster $\{P_2V_3W_{15}\}$ can also be grafted with an organic moiety via chelation of the TRIS moiety to the $\{V_3\}$ trimer cap[109] and Hasenknopf et al. have reported a series of POM hybrids of the type $[P_2V_3W_{15}O_{59}\{(OCH_2)_2C(Et)NHCOR\}]^{5-}$ which are the first examples of the insertion of amides into a POM framework cage. The interesting feature of these hybrids is the substitution of a POM oxo bridging ligand with the carbonyl oxygen of the amide function on the organic moiety. Variation of the amide residue allowed efficient electronic communication between the organic ligand and the inorganic cluster, which are reflected in the changes of redox properties of the hybrid POM. Conversely, the electron-accepting properties of the POM are transmitted to the ligand and this could be used to tune the organic part and help the design of POM-based redox sensors,[140,141] for light harvesting applications.[151]

As previously mentioned, there are many examples of hybrids incorporating d- or f-block metals, with recent examples reported by Mialane et al.,[152] where 3d transition-metal ions (Ni, Co, and Cu) and various carboxylic acid derivatives were combined under mild conditions to provide a novel 3d-metal hybrid compound (see **Figure 21**).

2.10.7 Frameworks

The number of reported open-framework (OF) inorganic materials has grown enormously since the 1990s. These consist mainly of MOFs with discrete inorganic building blocks. The nature of the building units determines the geometry and cavities of such frameworks.[153] For example, POM clusters can be used as large inorganic building blocks where the lattice of such framework materials can be expanded.[154] The 'shrink-wrapping' strategy combined with the 'building block approach'[37] and the choice of suitable linkers result in the creation of diverse polymeric architectures and robust framework materials incorporating some well-known POM building blocks, within the frame or within their cavities. Due to the large number of POM-based frameworks that can be designed, it is important to make the distinction between the POM-based open frameworks (POM–OFs: the POMs are part of the framework's skeleton)[37,55,155] and the POM-based metal–organic frameworks (POM–MOFs: the POMs are encapsulated in the pores of a MOF; see **Figure 22**).[156]

Author's personal copy

The assembly of purely inorganic POM-based porous frameworks is highly desirable in materials science, because they can combine the thermodynamic stability of zeolites and mesoporous silicas with the sophistication and versatility of MOFs.

2.10.7.1 POM-Based Frameworks

2.10.7.1.1 Silver as the transition-metal linker

The diverse geometries and bonding modes of Ag(I) make it a perfect linker in POM chemistry.[157] For example, Ag(I) salts have been condensed with β-octamolybdate anions as building units and bulky TBA as cations to create two 1D-chain isomeric structures.[49] In these 1D chains, the units $[Ag^{I}Mo^{VI}{}_{8}O_{26}Ag^{I}]^{2-}$ are almost totally enveloped by the flexible TBA cations, effectively isolating them from one another. The use of small cations instead of the large and flexible TBA cations reduces the steric shielding and/or the 'shrink-wrapping' effect leading to a partial disruption of the 'insulation.' For instance, a grid-like structure from the solvent dimethylsulfoxide (DMSO), and a 2D array in which the relatively bulky TBA ions are exchanged for HDMF cations were formed (HDMF = protonated dimethylformamide). In addition, the use of the bulky but rigid Ph_4P ions instead of TBA cations leads to a discrete cluster (see Figure 23).

Further studies on silver-octamolybdate systems focusing on the solvents and the counter-ion effects led to a new set of interesting POM-based architectures.[158] In these assemblies, the linker units $\{Ag_2\}$ and the fine-tuning of the Ag–Ag distances are achieved with the help of different coordinating solvents. A series of compounds based on silver-octamolybdate building blocks have been isolated, including an uncommon 0D, three 1D polymeric chains, and a 2D cross-linked network. Figure 23 shows some of these architectures, emphasizing the crucial roles of counter-ions and solvent molecules in their isolation. Therefore, these studies on silver-octamolybdate systems comprehensively illustrate the importance of the chosen synthetic strategies for the formation of structural assemblies with different dimensionalities. This behavior can be generalized to other metals. For example, silver cations can be directly coordinated to tungsten-based POMs, and a recent report showed that the Dawson-like POM $[H_4W_{19}O_{62}]^{6-}$ can be synthesized using the organic template TEAH (TEAH = protonated triethanolamine).[15] Precipitation with the TPA cation (TPA = *n*-tetrapropylammonium) leads to the isolation of two different isomers,[61] and these architectures appear to be controlled or directed by the nature of the atom within the POM which form different isomers. The two isolated isomers ($\{\alpha\text{-}W_{19}\}$ and $\{\gamma^{*}\text{-}W_{19}\}$) react in similar conditions in acetonitrile with $AgNO_3$ to form frameworks of different dimensionalities.

The isomer $\{\alpha\text{-}W_{19}\}$ (linked to 6 Ag(I)) leads to the formation of a 1D chain. In this structure, the silver connectors exhibit both the tetrahedral and linear geometries. In contrast to the $\{\gamma^{*}\text{-}W_{19}\}$ cluster (linked to 12 Ag(I)), the trimeric caps are not linked to Ag(I), and the chain is formed exclusively via silver bridges between the terminal oxygen on the central belt of the cluster. The second isomer is incorporated in a 3D framework via different silver coordination modes. Its central belt is linked to two dimeric $\{Ag_2\}$ units, in which the Ag(I) are fivefold coordinated in a distorted trigonal bipyramidal geometry. Subsequently, four $\{Ag_2\}$ dimers (with $d_{Ag-Ag} = 3.41$ Å) connect the trimeric cap to the belt of further clusters. Similarly, the Keggin-type isopolyoxotungstate $[H_4W_{12}O_{40}]^{4-}$ [155] forms in acetonitrile in the presence of $AgNO_3$ (Figure 24, bottom) a structure built from two protonated α-metatungstate clusters $\{W_{12}\}$ and dimeric $\{Ag_2\}$ bridging units. These building units are arranged

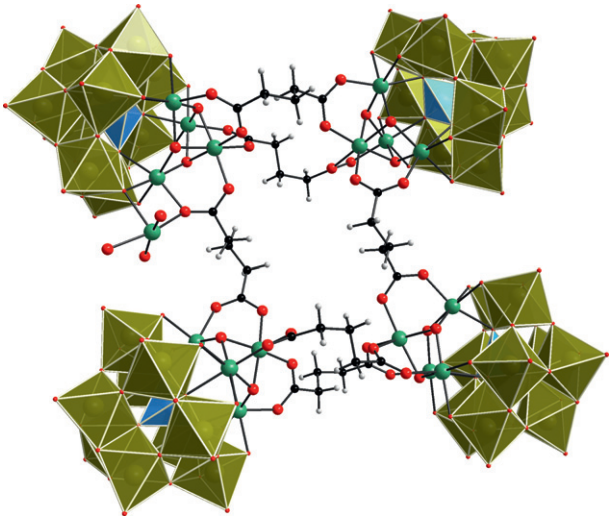

Figure 21 Mixed polyhedral and ball-and-stick representation of an $\{\alpha\text{-}SiW_9\}$ cluster. Color scheme: W, green (polyhedra); Si, blue (polyhedra); Ni, green; O, red; C, black; H, white.

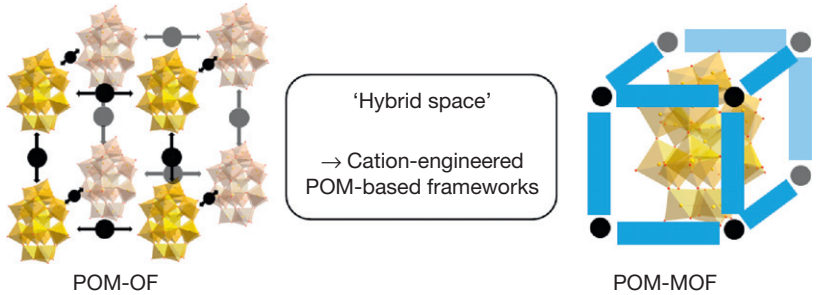

Figure 22 Left: In a POM–OF, the POM is linked iono-covalently by metallic cations; Middle: In cation-engineered POM frameworks, the organic cation wraps around the POM in such a way a 1D, 2D, or 3D framework is obtained. Right: The POM is inserted inside the cavity of an MOF during its synthesis or post-synthetically. The circles schematize the metallic cations, the arrows the iono-covalent interactions, and the blue rectangles the organic cations.

Author's personal copy

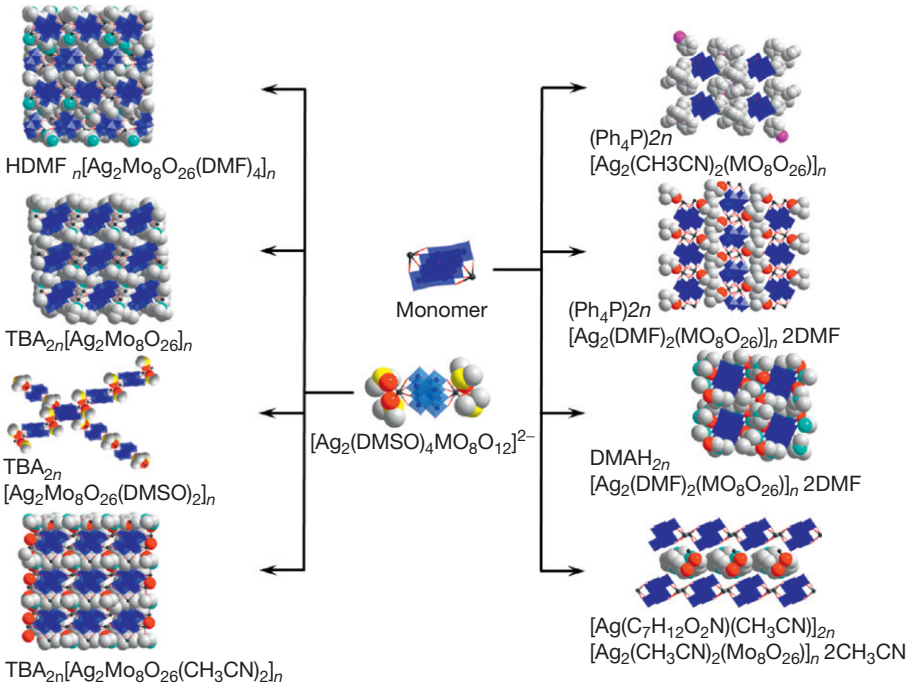

Figure 23 Summary of the structures isolated from the silver-octamolybdate reaction system. The solvents and counterions are represented in space-filling models to highlight their influence in determining the overall topologies Color scheme: Mo, blue (polyhedra); Ag, dark gray; S, yellow; P, pink; O, red; N, cyan; C, gray.

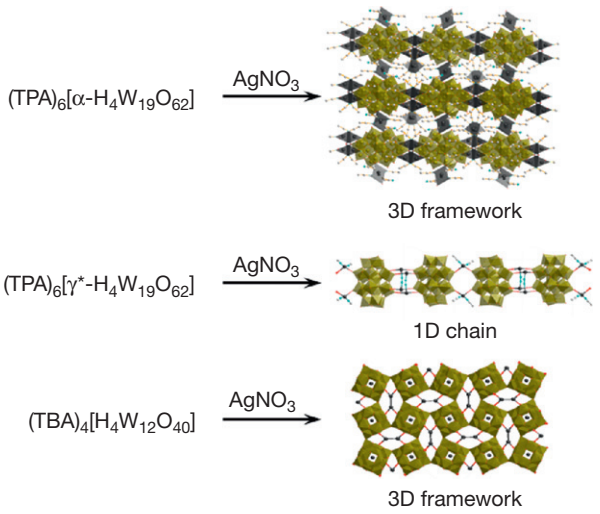

Figure 24 W-based POMs linked by silver cations. The counterions are not shown and the molecules of solvent coordinated to the silver on the bottom structure are hidden for clarity. Color scheme: W, green (polyhedra); O, red; Ag, dark gray; N, cyan; C, gray.

such as to enclose two sets of collinear channels in the crystal lattice. One important aspect of this framework formation is that argentophilic metal–metal interactions stabilize short silver–silver contacts allowing Ag^+ to self-organize into $\{Ag_2\}$ dimers, each of these motifs cross-linking four POM building blocks. In addition, coordinating solvents should be avoided to encourage the formation of the Ag–Ag interactions, since their use results in the capping of Ag centers yielding low dimensional structures. Nonclassical Dawson clusters can also be incorporated in frameworks using Ag(I) cations. For instance, $\{SbW_{18}\}$ and $\{BiW_{18}\}$ react with Ag(I) nitrate in acetonitrile in the presence of HNO_3 to form essentially isostructural framework materials.[159] These $\{SbW_{18}\}$ clusters are each coordinated to 12 silver cations and are positioned 'head to tail' in infinite pillars, which arrange in a hexagonal array; although being disordered, the silver positions reveal Ag–Ag interactions. It also appears crucial to the formation of the frameworks that the POM can adopt different degrees of protonation.

2.10.7.1.2 Nonsilver-based frameworks

A 3D inorganic framework, based on pure metal oxides and without the use of external linkers, has been obtained under strict pH control, reacting the divacant lacunary POM $[\gamma\text{-}SiW_{10}O_{36}]^{8-}$ with Mn(II) in the presence of morpholinium cations and potassium permanganate. This POM-based extended modular framework incorporates 'active sites' capable of responding to guest inclusion.[31,160] This pure metal-oxide framework based upon Mn-substituted Keggin-type POM building blocks encloses elliptical pockets of $26.85 \times 23.62 \times 12.93$ Å size, which encapsulate solvent molecules and morpholinium cations, Figure 25. This material, in addition to exhibiting unusual redox properties (see Section 2.10.8), can be repeatedly disassembled and reassembled without any structural change by dissolution in hot water followed by recrystallization.

A potentially very interesting aspect of the secondary building unit approach is the fact that true porous POM-based materials can be obtained from POM structures having a central open cavity. In this regard, the highly anionic POM $\{P_8W_{48}\}^{40-}$ is a perfect candidate, first because it incorporates a 1 nm diameter pore and second because it has the capability to extend into multidimensional architectures by electrophilic

Author's personal copy

functionalization of the outer sphere, as opposed to the internal cavity. Extending the building block approach further with this superlacunary polyoxoanion $[H_7P_8W_{48}O_{184}]^{33-}$ and transition-metal ions such as Co(II) as linkers, two cyclic cobalt-substituted heteropolyoxometalate frameworks have been synthesized under strict control of pH and buffer. In both frameworks, the central crown cavity of $\{P_8W_{48}\}$ is functionalized by a total of six Co(II) ions and additional Co(II) ions are grafted onto the outer rings extending the Co(II)–$\{P_8W_{48}\}$ anions into 1D chains in the former and into a 3D network in the latter.[161,162] Replacing the linker with the redox switchable Mn(II) cation in the presence of the salt LiOAc at the temperature 80 °C leads to an OF nanocube-based architecture. A careful tuning of the reaction conditions allows the ligation of a total of 24 manganese centers onto the outer regions of the $\{P_8W_{48}\}$ unit. Because of the cubic nature of the structure, eight Mn(II) cations are associated with each $\{P_8W_{48}\}$ building unit. The cavity of the pores is free of heavy metal atoms and contains only solvent molecules and some K^+ and Li^+ alkali-metal cations, which can be further exchanged by Cu^{2+}. Slight structural variations can be obtained by changing some synthetic parameters, (see Figure 26).

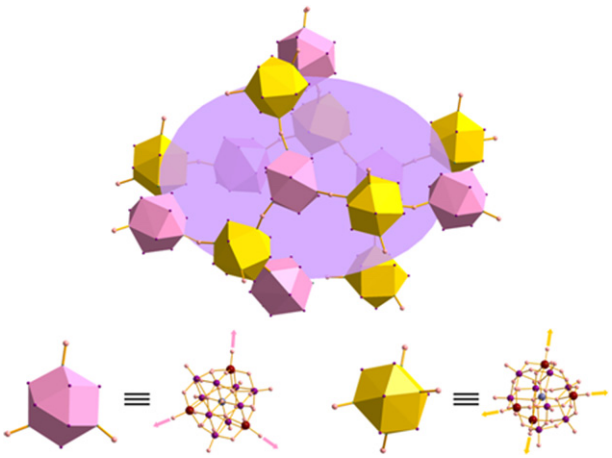

Figure 25 Illustration of the nanosized pockets in $[(C_4H_{10}NO)_{40}(W_{72}Mn_{12}O_{268}Si_7)_n]$ highlighted by the purple ellipsoid (dimensions: $\sim 2.7 \times 2.4 \times 1.3$ nm). The trigonal (rose) and tetrahedral (yellow) building block connectors are shown at the bottom; rose and yellow arrows highlight the connecting modes.

2.10.7.1.3 Hybrid frameworks

To illustrate the effect of the organic cations on the supramolecular structure of the POM frameworks, the case of the polyoxomolybdenum(V) phosphate clusters containing sodium-linked dimeric $\{Mo_6\}_2$ moieties as inorganic building blocks and the guanidinium cation, the 2-aminopyrimidinium cation, or the protonated ethylenediamine, respectively, as structure-directing amine cations has been investigated (Figure 27).[163] This results in the two rigid amine-based cations guanidinium and 2-aminopyrimidinium inducing the formation of layered arrangements, whereas the structurally more flexible ethylenediamine results in the formation of polymeric chains. This study is therefore the perfect illustration that the geometry, rigidity, and hydrogen bonding ability of organic cations can direct the overall structure of the POM supramolecular framework.

The transfer of properties from small building blocks to the large POM clusters is an interesting aspect in POM chemistry that is suitable for expansion and concrete development. For example, and as mentioned earlier, Hill and coworkers have achieved the chirality transfer from smaller enantiopure organic molecules such as tartrate onto POM clusters leading to chiral, nonracemizing, and enantiomerically pure polyoxotungstate clusters.[81] Extending this concept into large POM-based supramolecular frameworks, Cronin et al. have successfully developed a chiral framework material having sorption capabilities. Diprotonated (2)-sparteine has been used as the chiral cation and the dimeric polyoxomolybdenum(V) phosphate anion $[H_{15}Mo_{12}NaO_{62}P_8]^{8-}$ as the POM building block, resulting in a porous chiral hybrid framework.[79] In this framework, each dimeric $\{Mo_6\}$ POM cluster is shielded by four (2)-sparteine cations which form N–H···O hydrogen bonds to the cluster anion. The structure is further reinforced by a complex network of hydrogen-bonded water molecules and incorporates chiral channels capable of accommodating small organic molecules. The porous nature of

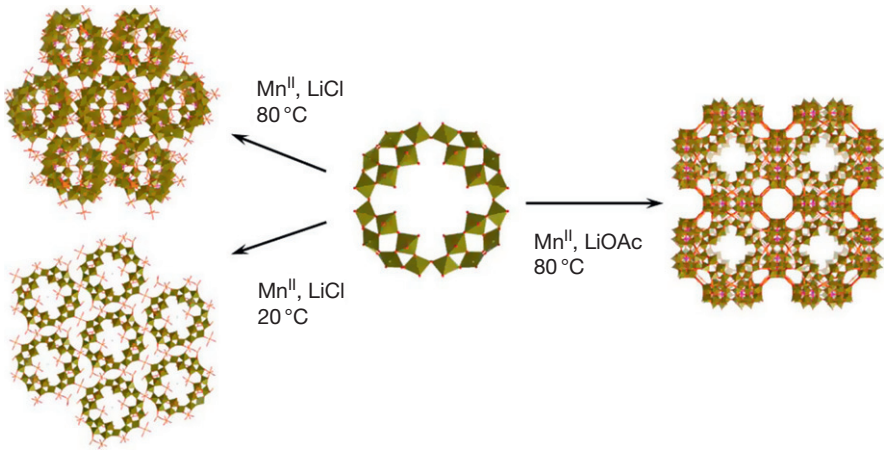

Figure 26 Representation of the synthetic procedure used to isolate the different Mn-$\{P_8W_{48}\}$-based POM–OFs. Color scheme: W, green (polyhedra); Mn, orange; P, pink; O, red.

Author's personal copy

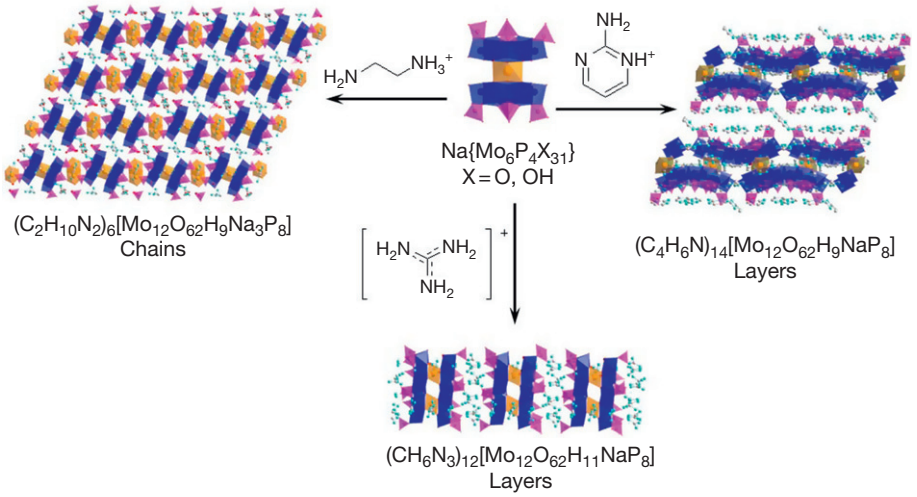

Figure 27 Summary of the formation of layered or chain-like structures from $\{Mo_6\}_2$ moieties depending on the amine used in the synthesis. Color scheme: Mo, blue (polyhedra); Na, light orange (polyhedra); O, red; P, pink; C, gray; N, cyan.

this compound is confirmed by reversible water sorption properties. In an attempt to develop POM-based chiral frameworks, large chiral metal–organic macrocations have also been used as one of the starting materials. Partly based on the work of Mizuno et al.,[164,165] an Fe-acrylate-based chiral macrocation is reacted and decomposes slowly with the trilacunary Dawson cluster $\{P_2W_{15}\}$. This helps to buffer the reaction medium leading to the formation of a nanosized tetrahedral polyoxotungstate molecule.[86,166] In the crystal lattice, the tetrahedral anionic cluster units are interconnected in a 3D network via external potassium ions. Looking for new organic cations to act as shrink-wrapping agents, BHEP has been used and is found to act as a tri-functional species being a cation, ligand, and buffer in POM synthesis. Two new POM architectures, the dimeric cluster unit $[\{PMnW_{11}O_{39}\}_2(PO_4)]^{13-}$ and a 2D network based on the $[P_2Mn_4W_{18}O_{68}]^{10-}$ anions, are isolated at pH 6.05 and 6.80, respectively, in the presence of the cation BHEP.[30,50–52] The dimeric cluster moieties are connected by a bridging phosphate unit that links the Mn(II) cationic centers attached to the monovacant Keggin entity. This moiety is stabilized in the solid state by the surrounding four H_2BHEP ions. Although the temperature and the pH have been only slightly increased to obtain the mentioned 2D network, this compound is entirely different from the dimeric cluster, consisting of two $\{PW_9O_{34}\}$ units sandwiching four manganese centers between them in a belt-like fashion. The important pH buffering capacity of the ligand BHEP is also revealed in the synthesis of three different Co(II)-containing silicotungstate clusters which have been observed before only as dimeric or higher-nuclearity complexes. The synthetic strategy employed involves the reaction of the Co(II) ions, the dilacunary $[\gamma\text{-}SiW_{10}O_{36}]^{8-}$ polyanion, and the bulky organic cation BHEP in basic media. Although the BHEP ligand is not incorporated in these structures, the fact that these clusters do not form in its absence proves that this amine ligand plays a vital buffering role in the isolation of these intermediate clusters.

2.10.7.2 POM–MOFs

MOFs are porous materials in which metals are linked to organic molecules in 3D arrangements. The size of the cavities can be tuned depending on the organic ligand. They are used mainly for gas storage, catalysis, separations, sensors, etc. MOFs are the object of extensive publications, and more information can be found in **Chapter 5.03** and elsewhere in this volume.[167–170] When the pore size of a MOF matches the size of a POM, it can be incorporated within the MOF postsynthetically, or during the formation of the MOF. In most cases, the POM is inserted after the isolation of the MOF. Férey et al. have reported the synthesis of the chromium/terephtalate-based MOF MIL-101, emphasizing two types of mesoporous cages with pore volumes of ~12 700 and ~20 600 Å^3.[171] The presence of different pore sizes could find some applications in the selective placement of guests. The incorporation of the Keggin anion $K_7PW_{11}O_{40}\cdot nH_2O$ (volume ~2250 Å^3) has been tested in that regard. They estimate that the large cages are occupied by an average of 5.3 Keggin anions. Kholdeeva et al. have reported the incorporation of Co- and Ti-substituted Keggin anions (e.g., $[PW_{11}CoO_{39}]^{5-}$ and $[PW_{11}TiO_{40}]^{5-}$) in MIL-101. This material exhibits good catalytic activity and selectivity in the allylic oxidation of α-pinene and caryophyllene epoxidation.[172] Similarly, polyoxotungstates $[PW_4O_{24}]^{3-}$ and $[PW_{12}O_{40}]^{3-}$ have been electrostatically attached to the surface of MIL-101. The resulting materials show similar catalytic activity toward alkene epoxidation compared to the 'free' POM in homogeneous conditions, but higher than the supported POM.[173] The MOF can also be built around the POM guest, as described by Hill et al.[156] When $Cu(NO_3)_2$, $K_5CuPW_{11}O_{39}$, and $(CH_3)_4NOH$ are reacted together it results in a structure where the surface area appears lower than most of the MOF pores, indicative of a high POM integration into the MOF. The POMs are accessible enough to be further involved in catalytic reactions and behave synergistically with the MOF for the oxidation of various thiol molecules, from H_2S to S_8.

2.10.8 Redox-Active POMs

The ability to configure or tailor redox properties is one of the most important features for POM compounds, and provides a

Author's personal copy

major motivation in the development of new functional systems. For example, the Dawson cluster, $\{Mo_{18}O_{62}X_2\}$, can be readily sixfold reduced without any change in the cluster geometry. Furthermore, the redox properties for the same type of clusters can be tuned by incorporating different heteroatoms or replacement of one metal ion on the cluster shell. For example, when the Dawson-type POMs are disubstituted with phenylphosphonate, phenylsilyl or tertbutylsilyl moieties, the resulting POM-hybrid can accept up to five electrons, and the organic substituents affect the first and second reduction potential of the POM compared to the unsubstituted $[P_2W_{18}O_{62}]^{6-}$. The presence of the phenyl-phosphonate lowers the reduction potential, whereas the phenyl silyl or the tertbutylsilyl moieties cause cathodic shifts.[174] The Preyssler anion, $[M^{n+}P_5W_{30}O_{110}]^{(15-n)-}$, features a rich chemistry shown by its ability to accept electrons at low potentials, to selectively capture various metal cations M^{n+}, and to undergo acid–base reactions. Theoretical calculations to evaluate the energetics of the release/encapsulation process for several M^{n+} cations and to identify the effect of the encapsulated ion on the properties of the Preyssler anion show a linear dependence between the first one-electron reduction energies and the encapsulated X^{n+} charge, with a slope of 48 mV per unit charge. The protonation also shifts the reduction potential to more positive values.[175] The first pure Keggin network $[\{W_{72}M_{12}O_{268}X_7\}_n]^{y-}$, where $M = Mn^{III}$, X = Si has been reported.[31] The repeat unit consists of two types of building blocks: three connected and four connected Keggin clusters linked via Mn–O–W bridges (see Figure 28). The 'active site' Mn(III) can chemically and reversibly be reduced in the solid state through single crystal to single crystal (SC–SC) transformation within 60 min. It is possible to follow the entire crystal oxidation–reduction by crystallography and the crystal structure remains nearly intact. Only the distance d_{Mn-W} between two clusters is changing, resulting in the expansion of the unit cell by 5.48% in volume (for the reduction process), and therefore a switchover of the electronic properties. The reverse reaction is also possible, both in solution (followed by subsequent recrystallization) and in the solid state. The change of oxidation state of the metal within the crystal can be monitored through the change of color of the crystals and further work has allowed the generalization of this new type of responsive materials.[160,176]

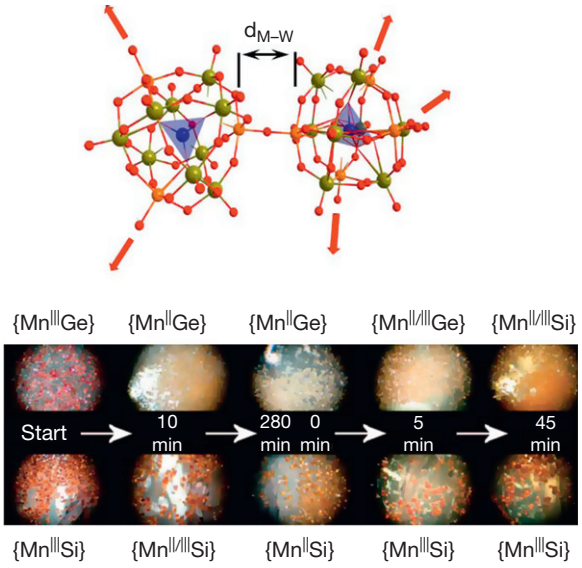

Figure 28 Redox switchable Keggin networks. Color scheme: W, green; W/Mn (50/50), orange; heteroatom (Si or Ge), blue (polyhedra); O, red.

Not only has the crystal structures of the 3D Keggin framework with the Si or the Ge heteroatoms and the Mn linkers been achieved, but it is also possible to change the Mn ions for Co ones which also shows switching between the Co+II and +III oxidation states. In general, d_{M-W} is smaller when M has the oxidation degree +III, and when M = Co. Surprisingly, the change of heteroatom has only a very small effect on d_{M-W} when M = Mn+II and +III. However, the biggest change due to the heteroatom is reported between $\{Co^{III}Ge\}$ (with $d_{M-W} = 3.44$ Å) and $\{Co^{III}Si\}$ ($d_{M-W} = 3.51$ Å). The largest difference in cell volume is noticed between $\{Mn^{II}Ge\}$ ($V = 60\,652$ Å^3) and $\{Co^{III}Ge\}$ ($V = 54\,955$ Å^3). Another consequence of the change of oxidation state is the change of color of the crystals (see Figure 28). It can indeed be visually noticed that the reduction of $\{Mn^{III}Ge\}$ to $\{Mn^{II}Ge\}$ is faster than the oxidation reaction, on the contrary to the reduction of $\{Mn^{III}Si\}$ to $\{Mn^{II}Si\}$, which is slower than the corresponding oxidation reaction. This is confirmed by the measured rate constants and shows nicely how the crystal-based oxidation and reduction reactions can have the kinetics tuned in either direction as a function of the embedded heteroanion. As the change of heterometal or/and heteroatom affects the physical properties of the framework, the assembly of mixtures of the isostructural frameworks or 'redox alloys' can be done, leading to a series of mixed Co/Mn POM-based networks and to the first example of POM alloys, and this opens the way for new materials with emergent properties.[176]

2.10.9 Devices, Catalysts, and Magnetism

2.10.9.1 Catalysis

The use of POM clusters as catalysts continues to be the most popular application area for POMs, especially in industry with hundreds of papers and many patents published every year covering this topic. There are many reviews that cover the progress of POM chemistry in this aspect. For most recent reviews see, for example, on the development of green H_2O_2-based epoxidation systems,[177] catalytic oxidation of organic substrates by molecular oxygen and hydrogen peroxide by multistep electron transfer – a biomimetic approach,[178] progress and challenges in POM-based catalysis and catalytic materials chemistry,[179] and catalytic strategies for sustainable oxidations in water.[180] For the purposes of this chapter, the focus will be only on important results published in the last few years. Catalysis with inorganic compounds is covered in Volume 6 of this series.

2.10.9.1.1 Water splitting

Efficient, catalytic water splitting is an important area of research, especially in the context of possible new energy developments for the utilization of solar energy (especially if the water splitting system can be embedded into photoelectrodes). As water oxidation involves a multielectron transfer process, the water splitting catalysts invariably include a transition metal in their structures. They can be differentiated in terms of their mode of action (homogeneous vs. heterogeneous) and also according to the kind of ligands coordinating

Author's personal copy

the redox-active transition metal (organic vs. inorganic) or their bonding pattern (framework vs. molecular). The design of water oxidation catalysts is challenging and to be viable they need to meet certain criteria (see Chapter 8.13). First they need to be stable toward oxidation, hydrolysis, and temperature.[181] They also need the capability of storing several electrons and should lead to energetically closed redox couples. Many studies have investigated the catalysts of different candidates. For instance, a fully inorganic redox-active POM (Figure 29) based upon a tetraruthenium POM $[\{Ru_4O_4(OH)_2(H_2O)_4\}(\gamma\text{-}SiW_{10}O_{36})_2]^{10-}$ combined with either a Ce(IV)[182] or a Ru $(bipy)_3^{3+}$ catalyst was found to catalyze the rapid oxidation of H_2O to O_2 in water at ambient temperature, with low overpotential and high turnover frequency.[183] This is thermodynamically the hardest part of the water splitting process. To complete the process, the conversion of protons to hydrogen is required so that the design of a POM-based hydrogen evolving complex and/or of a bi-functional system that could catalyze both processes would be interesting.

The exact reaction mechanism is currently the object of discussion. Bonchio et al.[184] and later Piccinin et al.[185] have reported computational works in order to elucidate the structural and electronic properties of the reaction intermediates of the structure shown in Figure 29. The main result is that the initial state (which is in an open-shell singlet) and the active state, which is supposed to promote water oxidation, have a difference of free energy lower than the thermodynamic limit for water oxidation, suggesting that this reaction would require cycling between higher oxidation states than Ru (IV)–OH/Ru(V)–OH. A variation of this reaction is found using a photogenerated species instead of the light source as shown in Figure 29. Bonchio et al.[186] have investigated the water oxidation by the photogenerated $Ru(Bipy)_3$ using the $[\{Ru_4O_4(OH)_2(H_2O)_4\}(\gamma\text{-}SiW_{10}O_{36})_2]^{10-}$ anion as a catalyst. They showed that the high negative charge of the $\{SiW_{10}\}$ moiety, combined with its structural rigidity that shields the Ru_4 core from the solvent, likely resulting in a very fast hole scavenging from the photogenerated Ru(III) complexes. This has been shown in homogeneous and heterogeneous (on TiO_2) conditions. The development of POM-based catalysts, multicentered and able to sustain multielectron transfer, is only at its early stage, and one of the most recent research topics consists of immobilizing them on an electroactive surface, to create new oxygen evolving centers (OECs).

2.10.9.1.2 Catalysts

Cationic crown-ether/POM ion pairs exhibit catalytic activities. The cation $[Pd(II)\{(H_3O)[15]crown\text{-}5\text{-}phen\}Cl_2]^-$ (phen = phenanthroline) and $[PV_2Mo_{10}O_{40}]^{5-}$ anion can catalyze Wacker-type alkene oxidation in essentially quantitative yields using N_2O instead of O_2 as the oxidant.[187] The hybrid complex $[Re(I)(15\text{-}crown\text{-}5\text{-}ether)(CO_3)CH_3CN\text{-}MHPW_{12}O_{40}]$ (with $M = Na^+$, H_3O^+) catalyzes the reduction of CO_2 to CO in the presence of H_2 under light.[188] Also, a hybrid carbon nanotube–POM can electrocatalytically oxidize methanol when the POM-modified carbon nanotube electrode is coated by Pt–Ru nanoparticles,[189] and the mechanism and kinetics of ether and alkanol cleavage catalyzed by POMs have been examined.[190] The phosphodiester bond cleavage by a POM was first reported using the heptamolybdate anion $[Mo_7O_{24}]^{6-}$. The reaction rate is accelerated by four orders of magnitude.[191,192] Ester hydrolysis in water can be greatly enhanced by the catalysis of the POM, $H_3PW_{12}O_{40}$, immobilized on organomodified mesoporous silica. This design overcomes the difficulty concerned with the use of solid acids whose catalytic activity is often severely deactivated by water.[193] The one-pot hydrogenolysis of glycol to the diol can be achieved with 96% selectivity to 1,2-PDO (PDO = propanediol) at 21% of glycerol conversion using a $Cs_{2.5}H_{0.5}[PW_{12}]$ catalyst with 5 wt% of ruthenium to give an active bi-functional catalytic system.[194] The di-copper-substituted γ-Keggin silicotungstate, $TBA_4[\gamma\text{-}H_2SiW_{10}O_{36}Cu_2(\mu_{1,1}\text{-}N_3)_2]$, is catalytically active in the oxidative alkyne homocoupling and formation of diynes from alkynes in good yields.[195] Dinuclear and tetranuclear metal sandwich-type silicotungstate clusters $[(\gamma\text{-}SiW_{10}O_{36})_2M_2(\mu\text{-}OH)_2]^{10-}$ and $[(\gamma\text{-}SiW_{10}O_{36})_2M_4(\mu_4\text{-}O)(\mu\text{-}OH)_6]^{8-}$ (M = Zr or Hf) show catalytic activity for the intramolecular cyclization of (+)-citronellal to isopulegols without formation of byproducts and it is suggested that the $[M_4(\mu_4\text{-}O)(\mu\text{-}OH)_6]^{8+}$ acts as an active site for the cyclization process.[196] A sandwich type γ-Keggin POM $TBA_8[\{Zn(OH_2)(\mu_3\text{-}OH)\}_2$

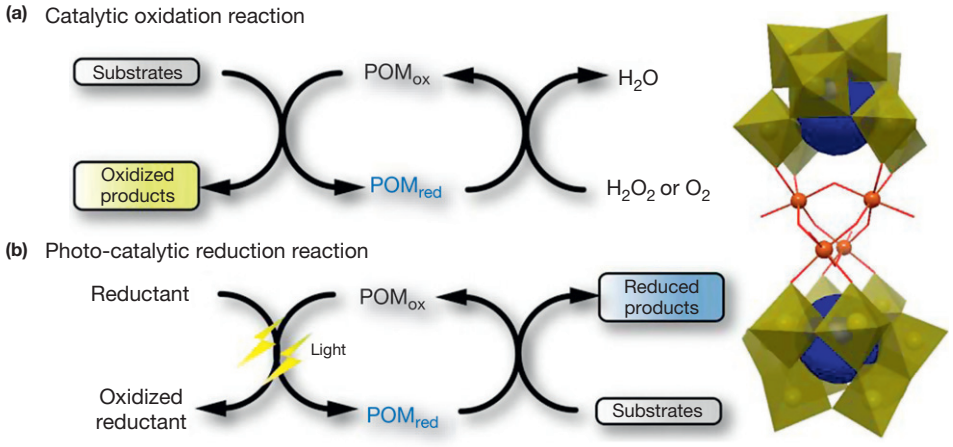

Figure 29 Left: POM-catalyzed reaction systems: catalytic oxidation reaction and photocatalytic reduction. Right: $\{Ru_4\}$-based POM catalyst. Color scheme: W, green (polyhedra); O, red; Si, dark blue; Ru, brown.

Author's personal copy

$\{Zn(OH_2)_2\{\gamma\text{-}HSiW_{10}O_{36}\}_2] \cdot 9H_2O$ catalyzes chemoselectively the oxidation of secondary alcohols in the presence of alkenic, alkynic, and primary alcohol functions.[197] A cesium salt of a divanadium-substituted phosphotuungstae $Cs_5[\gamma\text{-}PV_2W_{10}O_{40}]$ performs catalytically the hydroxylation of alkanes with a complete stereospecificity and regiospecificity.[198] The di-aluminum-substituted silicotungstate $TBA_3H[\gamma\text{-}SiW_{10}O_{36}\{Al(OH_2)\}_2(\mu\text{-}OH)_2]\cdot 4H_2O$ shows catalytic activity for the intramolecular cyclization of citronellal derivatives such as (+)-citronellal and 3-methylcitronellal without formation of byproducts.[199] POM–MOFs also show interesting catalytic properties. The POM-encapsulated MOF $([Cu_2(BTC)_{4/3}(H_2O)_2]_6[H_nXM_{12}O_{40}](C_4H_{12}N)_2$ (X = Si, Ge, P, As; M = W, Mo)), where the POM is alternately arranged without coordinative interactions, exhibits acid catalytic activity in the hydrolysis of esters, showing selectivity depending on the molecular size of substrates and their accessibility into the surface of the pore.[34] Further examples of POM–MOF-based catalyzes are provided in Section 2.10.7.2. Finally, $H_5PMo_{10}V_2O_{40}$ has been tested as a catalyst and a co-catalyst for methane oxidation in a microfluidic device, to implement genetic algorithms.[200]

2.10.9.2 Magnetism

POM clusters have a diverse range of electronic properties arising from the ability to form a set of reduced species and this feature, combined with the ability to act as well-defined ligands for polynuclear transition-metal clusters, means they have great potential for the discovery and design of new molecular magnetic devices. For instance, the $[PMo_{12}O_{40}(VO)_2]^{n-}$ cluster has been described as an important model compound as a possible spin qubit. This is because the redox-active core unit in the Keggin cluster is capped on opposed positions by two V=O species, each containing localized spin, that is, $s = 1/2$. It was then hypothesized that these two 1/2 spins can be coupled through the electrons of the central core by the electrical manipulation of the molecular redox potential due to the change of charge.[201] Also, the singularities of the POMs, such as the $\{Mo_{176}\}$ anion classified in the series of molybdenum blues, have been described in Section 2.10.4. In addition to its gigantic size, this nanowheel exhibits interesting electronic properties. Introducing magnetically active components to this structure could lead to interesting material. This has been done by using the cations Co(II) and Fe(III) to balance the charge of the structure. Indeed, the cluster $Na_{15}Fe_3Co_{16}[Mo_{176}O_{528}H_3(H_2O)_{80}]Cl_{27}\cdot 450H_2O$ has been characterized and as the Co cation is mainly high spin in that case, the whole structure exhibits a paramagnetic behavior.[202] Although the magnetic properties of polyoxovanadates have been well studied, new aspects continue to be discovered, for example, a recent example includes a theoretical study on the fully localized spin cluster of $[(V^{IV})_{18}O_{42}]^{12-}$ and its spin delocalized mixed-valence species $[V^{IV}{}_{10}V^{V}{}_8O_{42}]^{10-}$, which were reported based upon the structure of $Cs_{12}[V_{18}O_{42}(H_2O)]$.[203] Further, a series of compounds, $[V_6O_6(OCH_3)_8(calix)(CH_3OH)]$ anions (calix = p-*tert* butylcalix[4]arene), were synthesized using several organic cations (Et_4N^+, NH_4^+, PyH^+, and Et_3NH^+) by solvothermal reactions in methanol. The Lindqvist core was partially reduced and the composition of these clusters was shown to be $\{V^{III}V^{IV}{}_5O_{19}\}$, indicating a mixed-valence state. These compounds were the first polyoxovanadate-(III, IV) with a Lindqvist-type structure and ferromagnetic V(IV)...V(III) interactions as revealed by magnetic measurement.[204] In another example, the synthesis of a $\{Mn_{13}\}$ Keggin-like cluster is reported. The mixed valence of this complex allows switchable redox behavior, with its single-molecule magnet (SMM) properties being amplified as the cluster reaches a more oxidized state.[205]

Sandwich-based POMs where a metal 'core' is capped by POM ligands attract more and more attention since it is possible to introduce magnetic species into the POM using a 'designed' approach. Azide-based POM compounds with Mn(III) and Cu(II). as paramagnetic centers were reported where an end-to-end N_3^- bridging ligand acts as a linker between two $[(\gamma\text{-}SiW_{10}O_{36})Mn_2(OH)_2]^{4-}$ units and two $[\gamma\text{-}SiW_{10}O_{36}Cu_2(N_3)_2]^{6-}$ subunits connected through the two μ-1,1,1-azido ligands, with the four paramagnetic centers forming a lozenge. The azide ligands show different coupling properties depending on their conformation, end-to-end and end-on, which tend to lead to antiferromagnetic and ferromagnetic coupling, respectively.[206] Other Cu(II) clusters such as the sandwich-type POM cluster $\{Cu_8(GeW_9)_2\}$ show weak ferromagnetic exchange interactions among the Cu(II) centers.[207] In the sandwich-type POM $\{Cu_4(GeW_9)_2\}$, quantum tunneling at zero field is suggested from the asymmetric magnetization between a positive and a negative pulsed field at 0.5 K on the hysteresis loop.[208] Only a very few examples of POM-mediated SMMs are reported so far (see Figure 30). The cluster $[(GeW_9O_{34})_2(Mn^{III}{}_4Mn^{II}{}_2O_4(H_2O)_4)]^{12-}$ is one interesting example. A central cationic mixed-valence hexameric Mn core is stabilized by two POM ligands. Despite the complex and distorted nature of the cationic core, these architectures are very stable. The tetrahedral oxo ligands involved in the coordination to the transition-metal cationic core have an important role as the ideal tunable units to control/modify the physical properties of entire molecules.[209] It is also worth mentioning that a remarkable manganese cubane trapped by three inequivalent lacunary fragments has been reported. The complex $K_{18}[Mn^{III}{}_2Mn^{II}{}_4(\mu_3\text{-}O)_2(H_2O)_4(B\text{-}\beta\text{-}SiW_8O_{31})(B\text{-}\beta\text{-}SiW_9O_{34})(\gamma\text{-}SiW_{10}O_{36})]\cdot 40H_2O$ is composed of three different Keggin fragments ligating an appended $\{Mn_5\}$ cubane core. The stability of this structure is due to the fact that the Mn centers are inserted into the vacancies of the lacunary POMs.[210]

Other SMMs have also been reported – the $[ErW_{10}O_{36}]$ anion in which one Er ion is encapsulated by two $\{W_5\}$ ligands (Figure 30). The molecule is an inorganic analogue of the bis(phthalocyaninato)lanthanide SMMs. Both of them have a similar coordination/ligand field symmetries around the central Er ion where the distorted structure was also stabilized by the POM ligand.[211]

2.10.10 POM-Based Emergent Materials

The fact that POMs have high charges, well-defined structures, are based upon conserved building blocks, and form via self-assembly, means that they have great potential to bridge multiple length scales, see Figure 31. For instance, the $\{Mo_{154}\}$ wheel cluster, self-assembled at low pH under reducing

Author's personal copy

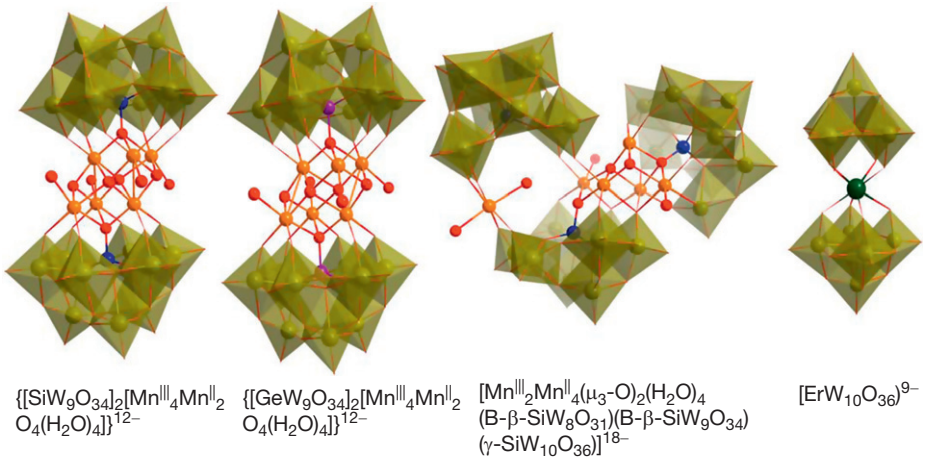

Figure 30 Structures of single-molecule magnets based on POMs. Color scheme: W (green), O (red), Mn (orange), Si (dark blue), Ge (violet), Er (dark green).

conditions from Na_2MoO_4, can undergo a further self-assembly process to form vesicle-like structures composed of ~1200 $\{Mo_{154}\}$ wheel-shaped clusters in solution.[212] Similarly, the cluster ball, $\{Mo_{72}Fe_{30}\}$, can also experience a self-assembly process to form spherical heteropolyoxometalate $\{Mo_{72}Fe_{30}\}$-based macro-ions which form single-layer vesicles (50–60 nm in diameter).[213] In addition to electrostatically assembled structures, the assembly of lacunary structures can result in nanosized compounds using transition-metal linkers, as well as the development of POM-mediated nanoparticle assemblies.

Many applications can be foreseen for POM-based nanostructures, particularly for nanotubes: containers, nanoreactors, conductors, etc. So far, different methods are available to fabricate POM-based nanotubes. Microtubes can be grown from $Ag_4SiW_{12}O_{40}$ in microemulsions in the presence of polyethyleneglycol[214]; $[(HTyr)_3XM_{12}O_{40}]$ (Tyr = tyrosine) tubes have been prepared in the solid state[215] and by template-free aqueous reaction of Keggin POMs.[216] The latter example highlights the importance of the cluster chosen for tube growth, since saturated species such as $\{\alpha\text{-}SiW_{12}\}$ grow solid rod structures whereas vacant species such as $\{\alpha\text{-}SiW_{11}\}$ or $\{\gamma\text{-}SiW_{10}\}$ grow nanotubes. It is worth mentioning that some of these materials (e.g., an ascorbic acid-doped $\{SiW_{12}\}$ tube) can be used as sensors, becoming blue upon exposure to ammonia, and as microreactors for the synthesis *in situ* of silver nanoparticles.[217] One of the interesting features of some of these materials is the possibility of switching between structures with different shapes.[218] $(DODA)_3PW_{12}O_{40}$ exhibits disk-like assemblies in a 3:1 mixture of chloroform and butanol. When the solvent ratio is 2:1, the disks disappear and instead conical structures with a hollow interior and lamellar walls, with a length of 1.5 μm, appear. In solution, the cones keep on growing and after 1–2 h of aging the cones reach up to 10 μm in length. Surprisingly, after 10 h in solution the cones aggregate to form disks again, which roll afterward into tubes. Another approach is to synthesize tubes by cation exchange. A hydrophobic hybrid POM has been obtained from the attachment of a polystyrene (PS) chain to $(TBA)_5[H_4P_2W_{15}V_3O_{62}]$, forming a transparent and homogeneous solution in DMF.[219] The addition of Dowex H^+ resin initiates the replacement of TBA^+ for H^+, thus

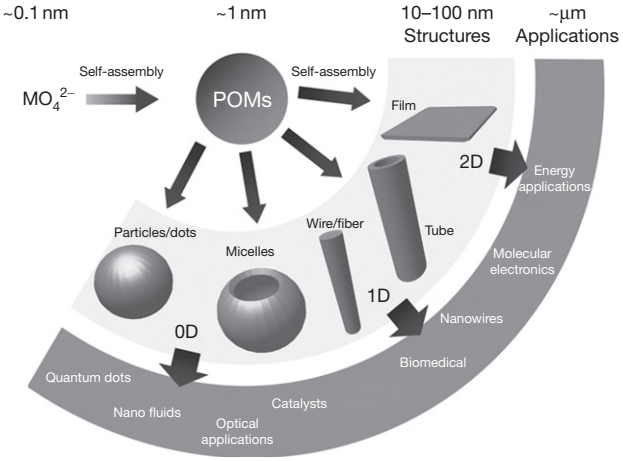

Figure 31 POM clusters (~1–5 nm in size) are assembled from mononuclear metal-oxide ions (~0.1 nm of size) and can also act as building blocks for nanoscale structures through template-mediated and electrostatic self-assemblies.

resulting in a turbid solution. Further analyses of the precipitate revealed the formation of the mixed hydrophilic H^+–POM head/hydrophobic PS tail arranged in reversed vesicles. After heating the sample at 70 °C for 12 h and aging at room temperature for 9 days, tubular structures start growing from the vesicles. After 14 days micelles are seen, arranged in a parallel fashion and exhibiting well-defined domains. The cation exchange can also take place at a solid–liquid interface. When a crystal of $[(C_4H_{10}NO)_{10}[W_{72}Mn_{12}O_{268}X_7]]_n$ (with X = Si, Ge) is submerged in water on a glass slide and then a bulky organic cation is added (dihydroimidazolphenanthridinium), the crystal slowly becomes encased in a membrane that ruptures under osmotic pressure and a tubular architecture grows from the crystal (**Figure 32**).[220] In addition, the size and growing direction seem easily tunable by playing with external factors. Such a versatile system could potentially be used as configurable microfluidic arrays. The same principle applied at liquid–liquid interfaces produces inorganic chemical cells (e.g., iCHELLs).[221]

Author's personal copy

2.10.10.1 Nanostructures by Cation Exchange

These examples of tube growth are all intriguing and because of the potential applications of such structures more work needs to be done to understand fully, and predict, these behaviors. Cronin et al. have published several studies aimed at a better understanding of their system, and so far no other cases of POM-based nanotubes are so well documented. The following sections offer a summary of their discoveries.

2.10.10.1.1 Tube growth at a solid–liquid interface

The transformation of POM crystals into tubular architectures occurs when a solution of a bulky cation is added to a slightly soluble crystal allowing it to dissolve locally, and producing an insoluble membrane by the electrostatic aggregation of the POM crystal and the bulky cation.[220] Once formed, the permeability of this membrane allows water to pass through and the osmotic pressure inside increases. When the system reaches a critical pressure, the membrane ruptures and the dissolved POM material contained within the membrane is ejected through the aperture, at which point it comes into contact with the cation solution, leading to the formation of an aggregate (see **Figure 32**) composed of the cations and POM anions bound electrostatically in a charge-balancing ratio.[222] The process of growth could theoretically allow a single tube to propagate until the crystal is entirely consumed; however, it often stops within 2–3 min (although growth can persist for as long as 30 min). This may be due to the pressure in the tube causing a new rupture point, either at the source or somewhere along the tube, in which case tube growth continues from that new rupture point and the original tube ceases to grow. The likelihood of this occurrence is increased when the growing end of the tube encounters an obstruction on the surface. This process is able to transform a large number of crystals simultaneously, and works for a wide range of POMs. Mixed tubes can also be fabricated simultaneously from different POMs.

The key properties of the POM crystals that influence the growth of tubes are their size and solubility as these govern both the amount of material that can be dissolved from the crystal surface and the rate at which it can aggregate. Once the tube growth has started, the limiting rate at which water can cross membrane, and therefore the rate of POM dissolution, becomes fixed and is related directly to the surface area of the membrane. If the membrane is weak or the dissolution of the crystal is too rapid (due to a too soluble crystal), there will not be sufficient containment to produce the required osmotic potential for tube growth. On the contrary, the tube growth will not initiate if the membrane is too strong to be broken by the osmotic pressure, or if the ruptures are instantly 'self-healed' due to a too high concentration in cation. If the pH of the solution is raised 'after' the tube growth initiation, the POM's solubility increases and therefore the growth rate increases. If the pH is raised 'before' the tube growth has started, the crystal dissolves too rapidly for the initial membrane shell to become consolidated and only precipitation is observed.[221] Any external factor such as the temperature or the pH affecting the solubility of the POM will also affect the growth process.

The properties of the cation and its local concentration must also be considered. For instance, in droplets the concentration change over time becomes significant and indeed tube diameter is seen to increase slightly. When the concentration of cation is truly maintained constant, no change in tube diameter is observed. In addition, the use of higher charged cations results in faster growing, narrowing the tubes since a lower local cation concentration is required in order to cause aggregation.[220] The concentration of cation allows one to control the diameter of tubes in 'real time' as well as its growth speed. Increasing the cation concentration leads to a decrease of the tube diameter and to faster growth, whereas the addition of pure water (to decrease the overall cation concentration) leads to an increase of the tube diameter and to slower growth (**Figure 33**).[221] This can be explained in terms of the availability of cations to reach a critical level of aggregation required for precipitation of the tube-forming material. In the limiting case, when the cation concentration is raised too far, tube growth

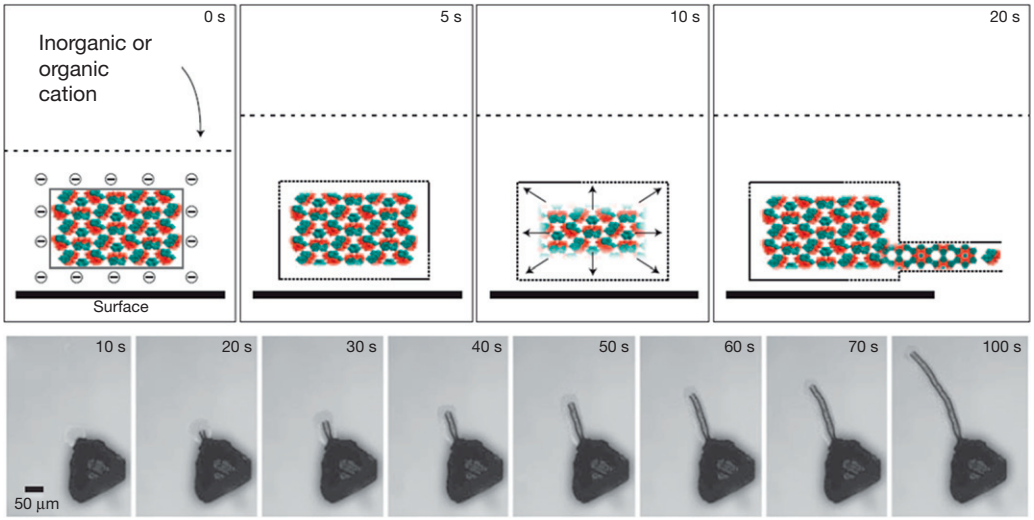

Figure 32 Scheme showing the transformation of crystals of POMs by cation exchange to tubular materials. Top: illustration showing how a cation added to a crystal in water causes the formation of a tube. Bottom: close-up of a single crystal over 100 s after addition of the cation.

Author's personal copy

will not propagate/initiate because any rupture in the membrane will be immediately sealed. In addition, the overall diameter and growth rate of the tubes are not altered by the changes in direction and this is consistent with a growth mechanism where the growth rate is determined by the surface area of the parent crystal and the concentration of available cations.[223]

Changing the ionic strength of a solution changes the osmotic pressure.[222] When a saturated aqueous solution of sodium chloride is added to a system where the tube growth has already started, the growth process is temporarily halted. On addition of the brine outside, the ionic strength of the solution is increased so that the osmotic potential across the membrane is reversed. The salt injection causes a second, competitive, osmotic pump to initiate, drawing solution into the membrane surrounding the crystal, through the tubes. This disrupts the osmotic growth mechanism, as no POM material can be ejected against this new flow direction. Once the concentration of NaCl inside the membrane and tube has been equilibrated, the original osmotic pump becomes predominant once again. The continued presence of NaCl however does change the solubility properties of the components and the aggregate, leading to significantly thicker/less consolidated tube walls.

Since an increase in temperature increases the POM solubility, a potential difference can be applied across opposite pairs of electrodes resulting in localized heating. Growing microtubes are observed to always alter their direction of growth so as to grow toward the cathode. A reduction in the lifetime of tube growth is observed due to the migration of the charged species toward the electrodes and a consequent reduction of concentration in the area in which direction control experiments are carried out.[223] In principle, it should be possible to direct the assembly of nanomolecular POM clusters to form microtubular architectures with a configurable composition, diameter, and orientation/shape.

2.10.10.1.2 Membrane growth at a liquid–liquid interface

In contrast to the formation of tubes at the solid–liquid interface by ion exchange, it is possible to form membranes at the liquid–liquid interface. This is done by injecting a solution of the ion pair 'POM–small cation' to a solution of 'large cation–small anion.' An 'extrusion-exchange' mechanism occurs in which the small cations associated with the POM are exchanged for the large organic cations, leading to an insoluble aggregate at the solution boundary (Figure 34).[221] The reverse process (e.g., a solution of the organic cation is injected in a solution of the POM) leads as well to the formation of the membrane. In practice, a micromanipulator needle is used to inject a solution of phosphotungstatic acid into a droplet of aqueous phenanthridinum cation, under an optical microscope.[224] The insoluble aggregate formed shows no permeability to the component species on either side of the membrane separating the initial solutions, thereby differing significantly from simple precipitate. They are flexible, encompassing sack-like architectures with controllable diameters comprised between 50 μm and several millimeters. These structures can be deflated and reinflated several times by drawing the contents back into the micromanipulator and then reinjecting. Several such architectures can coexist with one another, allowing bulk manufacture of sack structures, and they show no tendency to coalesce upon contact, instead remaining distinct entities. During the fabrication process, or when deliberately damaged, any ruptures in the membrane surface are immediately repaired as the two components come into contact with one another.

A large range of organic and inorganic cations can be used to form the membrane, from heterocylic derivatives of phenanthridiniums (DIPs) to the highly fluorescent $Ru^{II}(bipy)_3(BF_4)_2$ (bipy = 2,2′-bipyridyl) together with POMs with high structural diversity, from the $\{PW_{12}\}$ cluster and the phosphomolybdic acid ($H_3PMo_{12}O_{40}$, $\{PMo_{12}\}$) to more complex materials including the very large 3.6-nm wheel-shaped $\{Mo_{154}\}$ cluster. Membranous sack structures can also be produced in up to 1:1 water/acetonitrile mixtures and in aqueous ethanol solutions. The only requirement to this membrane's formation seems to be the necessity of using phosphate-based POMs. SEM of dried membranes shows small and slightly charged POM anions such as the 1.2 nm $\{PW_{12}\}$ (charged 3-) produce thinner

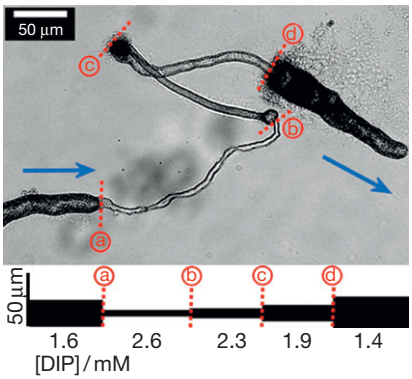

Figure 33 Size control of a growing tube by altering the available concentration of cations at points (a), (b), (c), and (d). The estimated concentrations and tube diameters at each point are shown in the lower section.

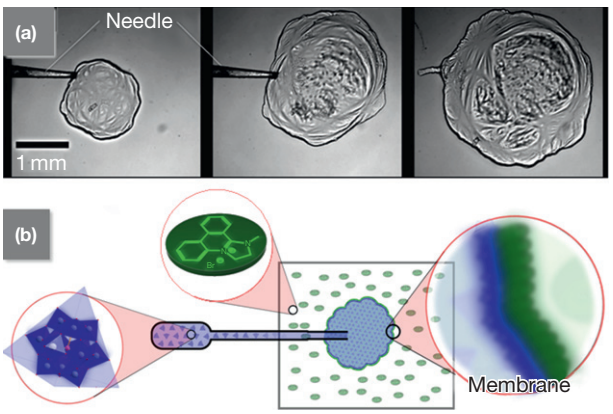

Figure 34 (a) A sequence of images showing the formation of a 1.2-mm diameter cell as the POM solution (phosphotungstic acid) is injected into the solution of the organic cation (methyl dihydroimidazophenanthridinium, DIP-Me). Needle aperture: ca. 20 mm. (b) Schematic illustration of the 'extrusion-exchange' mechanism of membrane formation. One component is injected into a solution of the other, in which cation exchange occurs on the POM, hence leading to aggregation.

Author's personal copy

(1–2 μm), more wrinkled, membrane surfaces, while higher sized and charged clusters such as the 1.8 nm $\{W_{48}\}$ (charged 40-) give much thicker and featureless membrane geography, although both types of membranes exhibit similar features. Cracks formed in the membranes show that their thickness can be up to 5 μm. A hypothesis is that the starting components aggregate in discrete charged-balance nanoparticles to form the membranes, where the particle size is controlled by the clusters sizes and charges. In addition, AFM studies show that a force of ~110 μN is exerted before the tip tears a $\{PW_{12}\}$-based membrane when it is derived from simple DIP–Me cations, suggesting a mechanical strength around 100 times weaker than a biological vesicle wall. A larger and more charged cation can increase the membranes' strength by ~15%, due to the enhanced cross-linking ability of the cation. The mechanical strength of these materials can therefore be controlled, which will be extremely useful when designing and building membrane-based devices.

2.10.10.2 Soluble Colloids

Understanding polyelectrolyte behavior in solution is still challenging, and, as such, aqueous solutions of highly charged and soluble POMs cannot be classified with simple ionic solutions which are well described by the Debye–Huckel theory, or with the charged colloidal particles, which are well described by the Derjaguin–Landau–Verwey–Overbeek theory.[225] In fact, as outlined in the previous sections, the behavior in solution of POMs is quite complex and they can be classified as strong electrolytes (macroions in solution) or weak electrolytes (locally negatively charged in solution, due to the deprotonation from the water ligands). Illustrations of this complex behavior are given by dynamic light scattering (DLS), static light scattering (SLS), and TEM experiments of large molecules such as $\{Mo_{154}\}$ in very dilute solution. The hydrodynamic radius is estimated to be at around 45 nm, which corresponds to approximately 1150 units. This suggests that the formation of vesicle-like hollow structures, with a single layered shell, is therefore different from surfactant assemblies. These so-called 'blackberry' structures are generally observed with POMs classified as strong electrolytes, and their size ranges from 20 to 1000 nm.[226] It is intriguing that such highly charged macroanions defy electrostatic repulsion and aggregate, even in dilute aqueous solution. However, when the solvent is pure acetone, the blackberry structures decompose. Changing the water content of the solvent mixture does not change the van der Waals forces, and it appears that the major driving force for the assembly of these hollow structures is the small counterion-mediated interaction.[227] Further DLS and SLS studies show that after dissolving the crystal in water, the monomeric units slowly aggregate in dimers and oligomers, the latter forming the blackberry structure in a fast step. It is possible to control the size of these structures by adjusting the solvent mixture, tuning the charge density either by using cationic surfactant or by changing the pH. The size of the vesicles can be predicted from the zeta potential and the cohesive bond energy, the size of the shell growing linearly with the inverse of the dielectric constant of the medium.[228] In contrast with cell membranes, these vesicles do not exhibit packed hydrophobic regions in the middle and therefore there is no need of ion channels for ion transport. Dye-based experiments show that the blackberry's membrane is permeable to small cations following a slow process, but not to anions.[229]

2.10.10.3 Hybrid-Based Nanostructures

2.10.10.3.1 Formation of vesicles

As explained in Section 2.10.6, the free amine of the Mn-Anderson can be involved in further reactions, and can react with acid chloride, acid groups, or aldehyde without affecting the inorganic moiety. When a hydrophobic alkyl chain is attached to the cluster via an amide bond, the resulting hybrid exhibits similar properties to those of surfactants, with the difference of incorporating a much larger inorganic polar headgroup. DLS and SLS studies show the formation of a supramolecular structure when the Mn-Anderson–C_{16} hybrid is solubilized in a solvent mixture MeCN/water with 35–60% of water.[230] The scattered intensity increases with time, consistent with the continuous formation of supramolecular structures. TEM studies show the formation of vesicles, which size range from 50 to 500 nm, depending on the solvent mixture constitution and the aging time. This size range is quite unusual for surfactants, for example, the lipid surfactant dipalmitoylphosphatidylcholine exhibits 10 nm large vesicles in aqueous solution. Contrary to the blackberry structures described earlier, only a small fraction of hybrids assemble into vesicles. It is understood that due to the large polar headgroup, the long alkyl chains have to bend into the solvo-phobic layer, which requires a high energy and therefore the bending curvature is small, forming large vesicles.

When the same hybrid is solubilized in the solvent mixture MeCN/toluene, solvophobic interactions are reversed and therefore the POMs assemble in reversed vesicles (see Figure 35). The size of the vesicles can be increased using higher amounts of toluene; however, there is no clear effect on the length of the alkyl chain.[124] The alkyl chain can be replaced by a photoswitchable organic moiety onto the Mn-Anderson. Wu et al. have attached an azobenzene to the tris connector of the hybrid POM.[231] When under visible light, the azo group adopts the *trans* isomer and forms fiber-like structures in MeOH/$CHCl_3$ solutions. Upon irradiation at 365 nm, the azo group isomerizes in the *cis* form, leading to the formation of sphere-like structures, as shown by SEM experiments. Hybrids can also be synthesized using the V-capped Wells–Dawson cluster $P_2V_3W_{15}$, which should lead to 'inorganic–organic–inorganic' hybrids with different surfactant properties. It has indeed been shown that such clusters form vesicle-like structures in mixtures of acetone/water, exhibiting an average size of 60–120 nm when increasing the concentration. The TBA counter-cations (ten per cluster) are expected to orient their alkyl chains in the solvophobic region, satisfying the requirements for vesicles' formation.[125] The organic linkers appear to play important roles in the formation/properties of the vesicles. The more hydrophobic, the more likely it is to observe monolayers at the interface. The vesicles' formation is an entropically favorable, charge-regulated process.[232]

2.10.10.3.2 Surface studies

POM-based monolayers on surfaces as well as multilayers generated by LB techniques and electrostatic layer-by-layer

Author's personal copy

assemblies have been studied from the 1990s, for their possible applications in a variety of fields such as catalysis and sensor systems. The majority of these studies are based on well-known structural archetypes such as the Keggin, the Dawson, and the Preyssler clusters and their lacunary and/or cation-exchanged derivatives. The potential for metal oxides to be applied in functional devices has revealed the need for further investigations of their self-assembly and organization in the solid state and on solid substrates. Recently, the focus has been shifted to the control of the physical and chemical parameters guiding the self-assembly and the self-organization of POMs on solid surfaces by solution processes. It was demonstrated by Cronin and Pignataro et al. that by simply employing drop-casting deposition of a selection of POM–organic hybrids it is possible to induce the formation of architectures with a wide variety of shapes and dimensionalities as a function of different parameters, such as the structure of the cluster, the nature of its functionalization, the solution concentration, and thermal treatment of the film.[130] The investigation of the self-assembly of hybrid organic–inorganic POMs is of immense interest due to the wide range of organic moieties with various functions that can be attached to (ligands), or associated with (cations), the inorganic metal core.[50,112,129,137]

In 2010, Cronin et al. presented an LB-induced surface study comparing three hybrid Mn-Anderson clusters, all as TBA salts, highlighting the strong relationship between the resulting surface architecture and the nature of the organic ligands functionalized on to the Mn-Anderson core.[112] Out of the three compounds investigated, the long-chain symmetrically functionalized Mn-Anderson, $(TBA)_3[(MnMo_6O_{18})((OCH_2)_3\text{-}C\text{-}(CH_2)_3CHCH_2)_2]$, did not result in any defined architectures. However, by changing the counter-cation from TBA to the surfactant dimethyldioctadecylammonium (DMDOA) well-defined 2D hexagonal nanostructures were obtained from LB deposition, highlighting the importance of the organic cation as well as the organic ligand, see Figure 36.[129] The hexagonal structures revealed fascinating dielectric behavior and reversible capacitive properties. The nanostructures are extremely stable under ambient conditions, and yet exhibit fascinating self-patterning upon heating. These findings present POMs as effective smart nanodielectrics and open up a new field for future POM applications.

2.10.11 Conclusion

It would seem that the possibility of applying these clusters into more and more areas of technology is really an interesting future prospect. Right now, metal oxides hold a special position in many functional materials from sunscreen to materials for complementary metal-oxide-semiconductors (CMOS) to

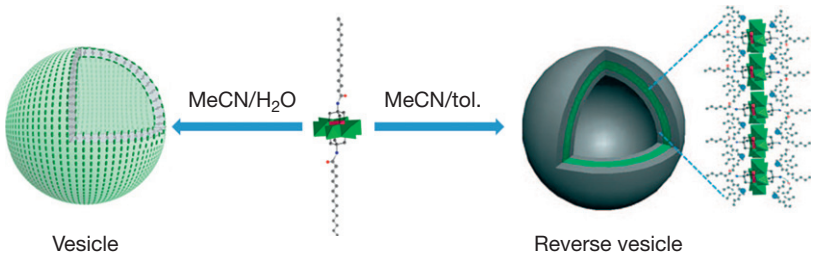

Figure 35 Vesicles' formation with the surfactant-like Mn-Anderson.

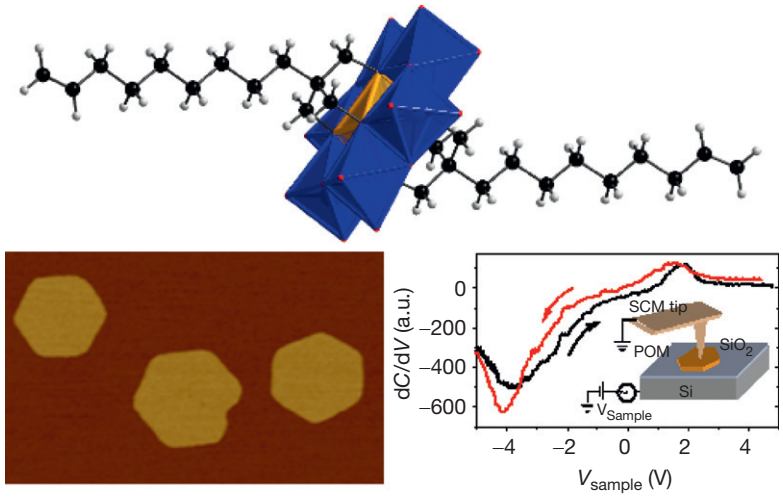

Figure 36 SFM images of $(NC_{38}H_{80})_3[(MnMo_6O_{18})((OCH_2)_3\text{-}C\text{-}(CH_2)_3CHCH_2)_2]$, resulting in uniform hexagonal nanostructures. Color scheme: Mo, blue (polyhedra); Mn, orange (polyhedra); O, red; C, black; H, white.

Author's personal copy

catalysis, and it will be interesting to see how POMs or molecular metal oxides can also be utilized in future technologies. Some of the challenges include the development of new energy materials (water splitting catalysts, batteries, and photoactive systems) and applications in electronics (sensors and information processing and storage) just to name a few from many emerging new possibilities. Such application goals will only be possible if a deep understanding of the structure/property relationship of this class of materials as well as a reliable and scalable route to manufacture is determined. Therefore, a good level of prediction of their shape via computational methods and fundamental research will have to be achieved. Improvements in processability, linked to the high charges associated with POMs, means that they could be trapped in polymeric, framework-based, or vesicle-like, matrices. By combining the synthetically adaptive chemistries with nano-to-micron scales, structures may allow a new way of arranging and developing functional systems. This could, in the broadest sense, show how inorganic chemistry really could come to life by allowing a new exploration of adaptive nanostructures based upon libraries of building blocks that can explored under far-from-equilibrium conditions.[233]

References

1. Long, D.-L.; Streb, C.; Kögerler, P.; *et al. J. Clust. Sci.* **2006**, *17*, 257–266.
2. Long, D.-L.; Tsunashima, R.; Cronin, L. *Angew. Chem. Int. Ed.* **2010**, *49*, 1736–1758.
3. Borras-Almenar, J. J., Coronado, E., Müller, A., et al. Eds.; *Polyoxometalate Molecular Science NATO Science Series II*. Kluwer Academic Dordrecht, 2003; Vol. 98.
4. Berzelius, J. J. *Poggend. Ann. Phys. Chem.* **1826**, *6*, 369.
5. Pauling, L. *J. Am. Chem. Soc.* **1929**, *51*, 1010–1026.
6. Gouzerh, P.; Che, M. *Actual. Chim.* **2006**, *298*, 9–22.
7. Werner, A. *Ber. Deutschen Chem. Ges.* **1907**, *40*, 40.
8. Laue, M.v. *Phys. Z.* **1913**, *14*, 1075.
9. Bragg, W. L. *Nature* **1912**, *90*, 410.
10. Keggin, J. F. *Nature* **1933**, *132*, 351.
11. Keggin, J. F. *Proc. R. Soc. Lond. A Mater.* **1934**, *144*, 75–100.
12. Pope, M. T.; Müller, A. *Angew. Chem. Int. Ed Engl.* **1991**, *30*, 34–48.
13. Hill, C. L. *Chem. Rev.* **1998**, *98*, 1–2.
14. Long, D.-L.; Burkholder, E.; Cronin, L. *Chem. Soc. Rev.* **2007**, *36*, 105–121.
15. Hasenknopf, B. *Front. Biosci.* **2005**, *10*, 275–287.
16. Song, Y.-F.; Long, D.-L.; Ritchie, C.; *et al. Chem. Rec.* **2011**, *11*, 158–171.
17. Miras, H. N.; Wilson, E. F.; Cronin, L. *Chem. Commun.* **2009**, 1297–1311.
18. Müller, A.; Roy, S. In: Oxomolybdates: *From Structures to Functions in a New Era of Nanochemistry*; Rao, A. M. C. N. R., Cheetham, A. K., Eds.; Wiley-VCH: Weinheim, 2004; Vol. II.
19. Vila-Nadal, L.; Wilson, E. F.; Miras, H. N.; *et al. Inorg. Chem.* **2011**, *50*, 7811–7819.
20. Pope, M. T., Ed.; In *Heteropoly and Isopoly Oxometalates*; Springer: Berlin, 1983; Vol. 8.
21. Ginsberg, E. A. P. *Inorg. Synth.* **1990**, *27*, 78–79.
22. Bassil, B. S.; Dickman, M. H.; Römer, I.; *et al. Angew. Chem. Int. Ed.* **2007**, *46*, 6192–6195.
23. Long, D.-L.; Orr, D.; Seeber, G.; *et al. J. Clust. Sci.* **2003**, *14*, 313–324.
24. Cronin, L. In *Comprehensive Coordination Chemistry II: From Biology to Nanotechnology*; McCleverty, J. A., Meyer, T. J., Eds.; Elsevier: Amsterdam, 2004; Vol. 7.
25. Long, D.-L.; Kögerler, P.; Farrugia, L. J.; *et al. Angew. Chem. Int. Ed.* **2003**, *42*, 4180–4183.
26. Long, D.-L.; Cronin, L. *Chem. Eur. J.* **2006**, *12*, 3698–3706.
27. Müller, A.; Krickemeyer, E.; Meyer, J.; *et al. Angew. Chem. Int. Ed Engl.* **1995**, *34*, 2122–2124.
28. Müller, A.; Krickemeyer, E.; Bögge, H.; *et al. Angew. Chem. Int. Ed.* **1998**, *37*, 3359–3363.
29. Yan, J.; Gao, J.; Long, D.-L.; *et al. J. Am. Chem. Soc.* **2010**, *132*, 11410–11411.
30. Ritchie, C.; Burkholder, E.; Kögerler, P.; *et al. Dalton Trans.* **2006**, 1712–1714.
31. Ritchie, C.; Streb, C.; Thiel, J.; *et al. Angew. Chem. Int. Ed.* **2008**, *47*, 6881–6884.
32. Fleming, C.; Long, D.-L.; McMillan, N.; *et al. Nature Nanotechnol.* **2008**, *3*, 229–233.
33. Himeno, S.; Katsuta, T.; Takamoto, M.; *et al. Bull. Chem. Soc. Jpn.* **2006**, *79*, 100–105.
34. Sun, C.-Y.; Liu, S.-X.; Liang, D.-D.; *et al. J. Am. Chem. Soc.* **2009**, *131*, 1883–1888.
35. Zou, N.; Chen, W. L.; Li, Y. G.; *et al. Inorg. Chem. Commun.* **2008**, *11*, 1367–1370.
36. Ammam, M.; Fransaer, J. *J. Solid State Chem.* **2011**, *184*, 818–824.
37. Pradeep, C. P.; Long, D.-L.; Cronin, L. *Dalton Trans.* **2010**, *39*, 9443–9457.
38. Contant, R. *Inorg. Synth.* **1990**, *27*, 104–111.
39. Contant, R.; Ciabrini, J.-P. *J. Chem. Res. Synop.* **1977**, 222.
40. Knoth, W. H.; Harlow, R. L. *J. Am. Chem. Soc.* **1981**, *103*, 1865–1867.
41. Canny, J.; Tézé, A.; Thouvenot, R.; *et al. Inorg. Chem.* **1986**, *25*, 2114–2119.
42. Kirby, J. F.; Baker, L. C. W. *Inorg. Chem.* **1998**, *37*, 5537–5543.
43. Long, D.-L.; Kögerler, P.; Cronin, L. *Angew. Chem. Int. Ed.* **2004**, *43*, 1817–1820.
44. Góral, M.; McCormac, T.; Dempsey, E.; *et al. Dalton Trans.* **2009**, 6727–6735.
45. Baffert, C.; Boas, J. F.; Bond, A. M.; *et al. Chem. Eur. J.* **2006**, *12*, 8472–8483.
46. Baffert, C.; Feldberg, S. W.; Bond, A. M.; *et al. Dalton Trans.* **2007**, 4599–4607.
47. Yan, J.; Long, D.-L.; Miras, H. N.; *et al. Inorg. Chem.* **2010**, *49*, 1819–1825.
48. Miras, H. N.; Stone, D. J.; McInnes, E. J. L.; *et al. Chem. Commun.* **2008**, 4703–4705.
49. Abbas, H.; Pickering, A. L.; Long, D.-L.; *et al. Chem. Eur. J.* **2005**, *11*, 1071–1078.
50. Ritchie, C.; Burkholder, E. M.; Long, D.-L.; *et al. Chem. Commun.* **2007**, 468–470.
51. Ritchie, C.; Li, F. Y.; Pradeep, C. P.; *et al. Dalton Trans.* **2009**, 6483–6486.
52. Ritchie, C.; Boyd, T.; Long, D.-L.; *et al. Dalton Trans.* **2009**, 1587–1592.
53. Bontchev, R. P.; Nyman, M. *Angew. Chem. Int. Ed.* **2006**, *45*, 6670–6672.
54. Niu, J. Y.; Ma, P. T.; Niu, H. Y.; *et al. Chem. Eur. J.* **2007**, *13*, 8739–8748.
55. Tsunashima, R.; Long, D.-L.; Miras, H. N.; *et al. Angew. Chem. Int. Ed.* **2010**, *49*, 113–116.
56. Ohlin, C. A.; Villa, E. M.; Fettinger, J. C.; *et al. Angew. Chem. Int. Ed.* **2008**, *47*, 5634–5636.
57. Nyman, M. *Dalton Trans.* **2011**, *40*, 8049–8058.
58. Hou, Y.; Nyman, M.; Rodriguez, M. A. *Angew. Chem. Int. Ed.* **2011**, *50*, 12514–12517.
59. Sigmon, G. E.; Unruh, D. K.; Ling, J.; *et al. Angew. Chem. Int. Ed.* **2009**, *48*, 2737–2740.
60. Sigmon, G. E.; Burns, P. C. *J. Am. Chem. Soc.* **2011**, *133*, 9137–9139.
61. Chubarova, E. V.; Dickman, M. H.; Keita, B.; *et al. Angew. Chem. Int. Ed.* **2008**, *47*, 9542–9546.
62. Xu, F.; Scullion, R. A.; Yan, J.; *et al. J. Am. Chem. Soc.* **2011**, *133*, 4684–4686.
63. Izarova, N. V.; Biboum, R. N.; Keita, B.; *et al. Dalton Trans.* **2009**, 9385–9387.
64. Delferro, M.; Graiff, C.; Elviri, L.; *et al. Dalton Trans.* **2010**, *39*, 4479–4481.
65. Izarova, N. V.; Vankova, N.; Banerjee, A.; *et al. Angew. Chem. Int. Ed.* **2010**, *49*, 7807–7811.
66. Barsukova-Stuckart, M.; Izarova, N. V.; Jameson, G. B.; *et al. Angew. Chem. Int. Ed.* **2011**, *50*, 2639–2642.
67. Pley, M.; Wickleder, M. S. *Angew. Chem. Int. Ed.* **2004**, *43*, 4168–4170.
68. Izarova, N. V.; Vankova, N.; Heine, T.; *et al. Angew. Chem. Int. Ed.* **2010**, *49*, 1886–1889.
69. Hill, C. L. *Nature* **2008**, *455*, 1045–1047.
70. Anderson, T. M.; Neiwert, W. A.; Kirk, M. L.; *et al. Science* **2004**, *306*, 2074–2077.
71. Kortz, U.; Lee, U.; Joo, H.-C.; *et al. Angew. Chem. Int. Ed.* **2008**, *47*, 9383–9384.
72. Cao, R.; Anderson, T. M.; Hillesheim, D. A.; *et al. Angew. Chem. Int. Ed.* **2008**, *47*, 9380–9382.
73. Anderson, T. M.; Cao, R.; Slonkina, E.; *et al. J. Am. Chem. Soc.* **2005**, *127*, 11948–11949.
74. Cao, R.; Anderson, T. M.; Piccoli, P. M. B.; *et al. J. Am. Chem. Soc.* **2007**, *129*, 11118–11133.
75. O'Halloran, K. P.; Zhao, C.; Ando, N. S.; *et al. Inorg. Chem.* **2012**, *51*, 7025–7031.
76. Barats, D.; Leitus, G.; Popovitz-Biro, R.; *et al. Angew. Chem. Int. Ed.* **2008**, *47*, 9908–9912.
77. Bassil, B. S.; Mal, S. S.; Dickman, M. H.; *et al. J. Am. Chem. Soc.* **2008**, *130*, 6696–6697.
78. Yan, L. K.; Lopez, X.; Carbo, J. J.; *et al. J. Am. Chem. Soc.* **2008**, *130*, 8223–8233.

Author's personal copy

79. Streb, C.; Long, D.-L.; Cronin, L. *Chem. Commun.* **2007**, 471–473.
80. Lan, Y. Q.; Li, S. L.; Su, Z. M.; *et al. Chem. Commun.* **2008**, 58–60.
81. Fang, X.; Anderson, T. M.; Hill, C. L. *Angew. Chem. Int. Ed.* **2005**, *44*, 3540–3544.
82. Zheng, X.; Zhang, L.; Li, J.; *et al. Chem. Commun.* **2011**, *47*, 12325–12327.
83. Thorimbert, S.; Hasenknopf, B.; Lacôte, E. *Isr. J. Chem.* **2011**, *51*, 275–280.
84. An, H.-Y.; Wang, E. B.; Xiao, D. R.; *et al. Angew. Chem. Int. Ed.* **2006**, *45*, 904–908.
85. Lan, Y. Q.; Li, S. L.; Wang, X. L.; *et al. Chem. Eur. J.* **2008**, *14*, 9999–10006.
86. Long, D.-L.; Kögerler, P.; Farrugia, L. J.; *et al. Chem. Asian J.* **2006**, *1*, 352–357.
87. Duval, S.; Floquet, S.; Simonnet-Jégat, C.; *et al. J. Am. Chem. Soc.* **2010**, *132*, 2069–2077.
88. Lemonnier, J.-F.; Duval, S.; Floquet, S.; *et al. Isr. J. Chem.* **2011**, *51*, 290–302.
89. Miras, H. N.; Zang, H. Y.; Long, D.-L.; *et al. Eur. J. Inorg. Chem.* **2011**, 5105–5111.
90. Korenev, V. S.; Boulay, A. G.; Dolbecq, A.; *et al. Inorg. Chem.* **2010**, *49*, 9740–9742.
91. Müller, A.; Serain, C. *Acc. Chem. Res.* **2000**, *33*, 2–10.
92. Müller, A.; Kögerler, P.; Dress, A. W. M. *Coord. Chem. Rev.* **2001**, *222*, 193–218.
93. Müller, A.; Kögerler, P. *Coord. Chem. Rev.* **2000**, *199*, 335–341.
94. Cronin, L.; Beugholt, C.; Müller, A. *J. Mol. Struct. Theochem.* **2000**, *500*, 181–193.
95. Müller, A.; Sarkar, S.; Shah, S. Q. N.; *et al. Angew. Chem. Int. Ed.* **1999**, *38*, 3238–3241.
96. Todea, A. M.; Merca, A.; Bögge, H.; *et al. Angew. Chem. Int. Ed.* **2007**, *46*, 6106–6110.
97. Müller, A.; Todea, A. M.; van Slageren, J.; *et al. Angew. Chem. Int. Ed.* **2005**, *44*, 3857–3861.
98. Müller, A.; Bögge, H.; Sousa, F. L.; *et al. Small* **2007**, *3*, 986–992.
99. Müller, A.; Shah, S. Q. N.; Bögge, H.; *et al. Angew. Chem. Int. Ed.* **2000**, *39*, 1614–1616.
100. Müller, A.; Beckmann, E.; Bögge, H.; *et al. Angew. Chem. Int. Ed.* **2002**, *41*, 1162–1167.
101. Müller, A.; Das, S. K.; Talismanov, S.; *et al. Angew. Chem. Int. Ed.* **2003**, *42*, 5039–5044.
102. Cronin, L.; Beugholt, C.; Krickemeyer, E.; *et al. Angew. Chem. Int. Ed.* **2002**, *41*, 2805–2808.
103. Thiel, J.; Yang, D.; Rosnes, M. H.; *et al. Angew. Chem. Int. Ed.* **2011**, *50*, 8871–8875.
104. Long, D.-L.; Streb, C.; Song, Y.-F.; *et al. J. Am. Chem. Soc.* **2008**, *130*, 1830–1832.
105. Miras, H. N.; Long, D.-L.; Kögerler, P.; *et al. Dalton Trans.* **2008**, 214–221.
106. Long, D.-L.; Kögerler, P.; Parenty, A. D. C.; *et al. Angew. Chem. Int. Ed.* **2006**, *45*, 4798–4803.
107. Long, D.-L.; Song, Y.-F.; Wilson, E. F.; *et al. Angew. Chem. Int. Ed.* **2008**, *47*, 4384–4387.
108. Miras, H. N.; Yan, J.; Long, D.-L.; *et al. Angew. Chem. Int. Ed.* **2008**, *47*, 8420–8423.
109. Pradeep, C. P.; Long, D.-L.; Newton, G. N.; *et al. Angew. Chem. Int. Ed.* **2008**, *47*, 4388–4391.
110. Wilson, E. F.; Abbas, H.; Duncombe, B. J.; *et al. J. Am. Chem. Soc.* **2008**, *130*, 13876–13884.
111. Wilson, E. F.; Miras, H. N.; Rosnes, M. H.; *et al. Angew. Chem. Int. Ed.* **2011**, *50*, 3720–3724.
112. Rosnes, M. H.; Musumeci, C.; Pradeep, C. P.; *et al. J. Am. Chem. Soc.* **2010**, *132*, 15490–15492.
113. Song, Y.-F.; Long, D.-L.; Kelly, S. E.; *et al. Inorg. Chem.* **2008**, *47*, 9137–9139.
114. Ma, M. T.; Waters, T.; Beyer, K.; *et al. Inorg. Chem.* **2009**, *48*, 598–606.
115. Ohlin, C. A.; Villa, E. M.; Fettinger, J. C.; *et al. Angew. Chem. Int. Ed.* **2008**, *47*, 8251–8254.
116. Sakamoto, S.; Fujita, M.; Kim, K.; *et al. Tetrahedron* **2000**, *56*, 955–964.
117. Yan, J.; Long, D.-L.; Wilson, E. F.; *et al. Angew. Chem. Int. Ed.* **2009**, *48*, 4376–4380.
118. Kistler, M. L.; Bhatt, A.; Liu, G.; *et al. J. Am. Chem. Soc.* **2007**, *129*, 6453–6460.
119. Smith, D. P.; Knapman, T. W.; Campuzano, I.; *et al. Eur. J. Mass. Spectrom.* **2009**, *15*, 113–130.
120. Kanu, A. B.; Dwivedi, P.; Tam, M.; *et al. J. Mass Spectrom.* **2008**, *43*, 1–22.
121. Brocker, E. R.; Anderson, S. E.; Northrop, B. H.; *et al. J. Am. Chem. Soc.* **2010**, *132*, 13486–13494.
122. Dolbecq, A.; Dumas, E.; Mayer, C. R.; *et al. Chem. Rev.* **2010**, *110*, 6009–6048.
123. Proust, A.; Thouvenot, R.; Gouzerh, P. *Chem. Commun.* **2008**, 1837–1852.
124. Zhang, J.; Song, Y.-F.; Cronin, L.; *et al. Chem. Eur. J.* **2010**, *16*, 11320–11324.
125. Pradeep, C. P.; Misdrahi, M. F.; Li, F. Y.; *et al. Angew. Chem. Int. Ed.* **2009**, *48*, 8309–8313.
126. Peng, J.; Ma, H.-Y.; Han, Z.-G.; *et al. Dalton Trans.* **2003**, 3850–3855.
127. Ito, T.; Yamase, T. *Eur. J. Inorg. Chem.* **2009**, 5205–5210.
128. Tsunashima, R.; Richmond, C.; Cronin, L. *Chem. Sci.* **2012**, *3*, 343–348.
129. Musumeci, C.; Rosnes, M. H.; Giannazzo, F.; *et al. ACS Nano* **2011**, *5*, 9992–9999.
130. Musumeci, C.; Luzio, A.; Pradeep, C. P.; *et al. J. Phys. Chem. C* **2011**, *115*, 4446–4455.
131. Song, Y.-F.; McMillan, N.; Long, D.-L.; *et al. Chem. Eur. J.* **2008**, *14*, 2349–2354.
132. Kaba, M. S.; Song, I. K.; Duncan, D. C.; *et al. Inorg. Chem.* **1998**, *37*, 398–406.
133. Polarz, S.; Smarsly, B.; Antonietti, M. *Chemphyschem* **2001**, *2*, 457–461.
134. Gouzerh, P.; Proust, A. *Chem. Rev.* **1998**, *98*, 77–111.
135. Proust, A.; Gouzerh, P.; Robert, F. *Inorg. Chem.* **1993**, *32*, 5291–5298.
136. Li, D.; Song, J.; Yin, P.; *et al. J. Am. Chem. Soc.* **2011**, *133*, 14010–14016.
137. Song, Y.-F.; Long, D.-L.; Cronin, L. *Angew. Chem. Int. Ed.* **2007**, *46*, 3900–3904.
138. Moore, A. R.; Kwen, H.; Beatty, A. M.; *et al. Chem. Commun.* **2000**, 1793–1794.
139. Hasenknopf, B.; Delmont, R.; Herson, P.; *et al. Eur. J. Inorg. Chem.* **2002**, 1081–1087.
140. Li, J.; Huth, I.; Chamoreau, L. M.; *et al. Angew. Chem. Int. Ed.* **2009**, *48*, 2035–2038.
141. Oble, J.; Riflade, B.; Noël, A.; *et al. Org. Lett.* **2011**, *13*, 5990–5993.
142. Peng, Z. H. *Angew. Chem. Int. Ed.* **2004**, *43*, 930–935.
143. Hao, J.; Xia, Y.; Wang, L. S.; *et al. Angew. Chem. Int. Ed.* **2008**, *47*, 2626–2630.
144. Wilson, A. J.; Robinson, W. T.; Wilkins, C. J. *Acta Crystallogr. C* **1983**, *39*, 54–56.
145. Chen, Q.; Zubieta, J. *Inorg. Chem.* **1990**, *29*, 1456–1458.
146. Müller, A.; Meyer, J.; Bögge, H.; *et al. Chem. Eur. J.* **1998**, *4*, 1388–1397.
147. Chen, Q.; Goshorn, D. P.; Scholes, C. P.; *et al. J. Am. Chem. Soc.* **1992**, *114*, 4667–4681.
148. Wu, P.; Yin, P.; Zhang, J.; *et al. Chem. Eur. J.* **2011**, *17*, 12002–12005.
149. Zhang, J.; Hao, J.; Wei, Y.; *et al. J. Am. Chem. Soc.* **2010**, *132*, 14–15.
150. Wu, P.; Xiao, Z.; Zhang, J.; *et al. Chem. Commun.* **2011**, *47*, 5557–5559.
151. Odobel, F.; Séverac, M.; Pellegrin, Y.; *et al. Chem. Eur. J.* **2009**, *15*, 3130–3138.
152. Rousseau, G.; Oms, O.; Dolbecq, A.; *et al. Inorg. Chem.* **2011**, *50*, 7376–7378.
153. Cheetham, A. K.; Férey, G.; Loiseau, T. *Angew. Chem. Int. Ed.* **1999**, *38*, 3268–3292.
154. Marleny Rodriguez-Albelo, L.; Ruiz-Salvador, A. R.; Sampieri, A.; *et al. J. Am. Chem. Soc.* **2009**, *131*, 16078–16087.
155. Streb, C.; Ritchie, C.; Long, D.-L.; *et al. Angew. Chem. Int. Ed.* **2007**, *46*, 7579–7582.
156. Song, J.; Luo, Z.; Britt, D. K.; *et al. J. Am. Chem. Soc.* **2011**, *133*, 16839–16846.
157. Villanneau, R.; Proust, A.; Robert, F. *Chem. Commun.* **1998**, 1491–1492.
158. Abbas, H.; Streb, C.; Pickering, A. L.; *et al. Cryst. Growth Des.* **2008**, *8*, 635–642.
159. McGlone, T.; Streb, C.; Busquets-Fité, M.; *et al. Cryst. Growth Des.* **2011**, *11*, 2471–2478.
160. Thiel, J.; Ritchie, C.; Streb, C.; *et al. J. Am. Chem. Soc.* **2009**, *131*, 4180–4181.
161. Mitchell, S. G.; Gabb, D.; Ritchie, C.; *et al. CrystEngComm* **2009**, *11*, 36–39.
162. Mitchell, S. G.; Streb, C.; Miras, H. N.; *et al. Nature Chem.* **2010**, *2*, 308–312.
163. Streb, C.; Long, D.-L.; Cronin, L. *CrystEngComm* **2006**, *8*, 629–634.
164. Uchida, S.; Hashimoto, M.; Mizuno, N. *Angew. Chem. Int. Ed.* **2002**, *41*, 2814–2817.
165. Uchida, S.; Mizuno, N. *J. Am. Chem. Soc.* **2004**, *126*, 1602–1603.
166. Pradeep, C. P.; Long, D.-L.; Kögerler, P.; *et al. Chem. Commun.* **2007**, 4254–4256.
167. Kitagawa, S.; Kitaura, R.; Noro, S. *Angew. Chem. Int. Ed.* **2004**, *43*, 2334–2375.
168. Yaghi, O. M.; O'Keeffe, M.; Ockwig, N. W.; *et al. Nature* **2003**, *423*, 705–714.
169. Eddaoudi, M.; Moler, D. B.; Li, H. L.; *et al. Acc. Chem. Res.* **2001**, *34*, 319–330.
170. Batten, S. R.; Robson, R. *Angew. Chem. Int. Ed.* **1998**, *37*, 1460–1494.
171. Férey, G.; Mellot-Draznieks, C.; Serre, C.; *et al. Science* **2005**, *309*, 2040–2042.
172. Maksimchuk, N. V.; Timofeeva, M. N.; Melgunov, M. S.; *et al. J. Catal.* **2008**, *257*, 315–323.
173. Maksimchuk, N. V.; Kovalenko, K. A.; Arzumanov, S. S.; *et al. Inorg. Chem.* **2010**, *49*, 2920–2930.
174. Boujtita, M.; Boixel, J.; Blart, E.; *et al. Polyhedron* **2008**, *27*, 688–692.
175. Fernandez, J. A.; López, X.; Bo, C.; *et al. J. Am. Chem. Soc.* **2007**, *129*, 12244–12253.
176. Thiel, J.; Ritchie, C.; Miras, H. N.; *et al. Angew. Chem. Int. Ed.* **2010**, *49*, 6984–6988.
177. Mizuno, N.; Yamaguchi, K. *Chem. Rec.* **2006**, *6*, 12–22.

Author's personal copy

178. Piera, J.; Bäckvall, J. E. *Angew. Chem. Int. Ed.* **2008**, *47*, 3506–3523.
179. Hill, C. L. *J. Mol. Catal. A: Chem.* **2007**, *262*, 2–6.
180. Carraro, M.; Sartorel, A.; Scorrano, G.; *et al. Synthesis* **2008**, 1971–1978.
181. Geletii, Y. V.; Yin, Q.; Hou, Y.; *et al. Isr. J. Chem.* **2011**, *51*, 238–246.
182. Sartorel, A.; Carraro, M.; Scorrano, G.; *et al. J. Am. Chem. Soc.* **2008**, *130*, 5006–5007.
183. Geletii, Y. V.; Botar, B.; Kögerler, P.; *et al. Angew. Chem. Int. Ed.* **2008**, *47*, 3896–3899.
184. Sartorel, A.; Miró, P.; Salvadori, E.; *et al. J. Am. Chem. Soc.* **2009**, *131*, 16051–16053.
185. Piccinin, S.; Fabris, S. *Phys. Chem. Chem. Phys.* **2011**, *13*, 7666–7674.
186. Orlandi, M.; Argazzi, R.; Sartorel, A.; *et al. Chem. Commun.* **2010**, *46*, 3152–3154.
187. Ettedgui, J.; Neumann, R. *J. Am. Chem. Soc.* **2009**, *131*, 4–5.
188. Ettedgui, J.; Diskin-Posner, Y.; Weiner, L.; *et al. J. Am. Chem. Soc.* **2011**, *133*, 188–190.
189. Pan, D. W.; Chen, J. H.; Tao, W. Y.; *et al. Langmuir* **2006**, *22*, 5872–5876.
190. Macht, J.; Janik, M. J.; Neurock, M.; *et al. J. Am. Chem. Soc.* **2008**, *130*, 10369–10379.
191. Cartuyvels, E.; Absillis, G.; Parac-Vogt, T. N. *Chem. Commun.* **2008**, 85–87.
192. Absillis, G.; Cartuyvels, E.; Van Deun, R.; *et al. J. Am. Chem. Soc.* **2008**, *130*, 17400–17408.
193. Inumaru, K.; Ishihara, T.; Kamiya, Y.; *et al. Angew. Chem. Int. Ed.* **2007**, *46*, 7625–7628.
194. Alhanash, A.; Kozhevnikova, E. F.; Kozhevnikov, I. V. *Catal. Lett.* **2008**, *120*, 307–311.
195. Kamata, K.; Yamaguchi, S.; Kotani, M.; *et al. Angew. Chem. Int. Ed.* **2008**, *47*, 2407–2410.
196. Kikukawa, Y.; Yamaguchi, S.; Tsuchida, K.; *et al. J. Am. Chem. Soc.* **2008**, *130*, 5472–5478.
197. Kikukawa, Y.; Yamaguchi, K.; Mizuno, N. *Angew. Chem. Int. Ed.* **2010**, *49*, 6096–6100.
198. Kamata, K.; Yonehara, K.; Nakagawa, Y.; *et al. Nature Chem.* **2010**, *2*, 478–483.
199. Kikukawa, Y.; Yamaguchi, S.; Nakagawa, Y.; *et al. J. Am. Chem. Soc.* **2008**, *130*, 15872–15878.
200. Kreutz, J. E.; Shukhaev, A.; Du, W.; *et al. J. Am. Chem. Soc.* **2010**, *132*, 3128–3132.
201. Lehmann, J.; Gaita-Arino, A.; Coronado, E.; *et al. Nature Nanotechnol.* **2007**, *2*, 312–317.
202. Imai, H.; Akutagawa, T.; Kudo, F.; *et al. J. Am. Chem. Soc.* **2009**, *131*, 13578–13579.
203. Calzado, C. J.; Clemente-Juan, J. M.; Coronado, E.; *et al. Inorg. Chem.* **2008**, *47*, 5889–5901.
204. Aronica, C.; Chastanet, G.; Zueva, E.; *et al. J. Am. Chem. Soc.* **2008**, *130*, 2365–2371.
205. Newton, G. N.; Yamashita, S.; Hasumi, K.; *et al. Angew. Chem. Int. Ed.* **2011**, *50*, 5716–5720.
206. Mialane, P.; Duboc, C.; Marrot, J.; *et al. Chem. Eur. J.* **2006**, *12*, 1950–1959.
207. Zhao, J. W.; Zhang, J.; Zheng, S. T.; *et al. Chem. Commun.* **2008**, 570–572.
208. Yamase, T.; Abe, H.; Ishikawa, E.; *et al. Inorg. Chem.* **2009**, *48*, 138–148.
209. Ritchie, C.; Ferguson, A.; Nojiri, H.; *et al. Angew. Chem. Int. Ed.* **2008**, *47*, 5609–5612.
210. Mitchell, S. G.; Molina, P. I.; Khanra, S.; *et al. Angew. Chem. Int. Ed.* **2011**, *50*, 9154–9157.
211. AlDamen, M. A.; Clemente-Juan, J. M.; Coronado, E.; *et al. J. Am. Chem. Soc.* **2008**, *130*, 8874–8875.
212. Liu, T. B.; Diemann, E.; Li, H. L.; *et al. Nature* **2003**, *426*, 59–62.
213. Liu, G.; Liu, T. B. *Langmuir* **2005**, *21*, 2713–2720.
214. Kang, Z.; Wang, E. B.; Jiang, M.; *et al. Eur. J. Inorg. Chem.* **2003**, 370–376.
215. Wang, R. Y.; Jia, D. Z.; Zhang, L.; *et al. Adv. Funct. Mater.* **2006**, *16*, 687–692.
216. Xin, Z.; Peng, J.; Wang, T.; *et al. Inorg. Chem.* **2006**, *45*, 8856–8858.
217. Shen, Y.; Peng, J.; Pang, H.; *et al. Chem. Eur. J.* **2011**, *17*, 3657–3662.
218. Nisar, A.; Zhuang, J.; Wang, X. *Chem. Mater.* **2009**, *21*, 3745–3751.
219. Han, Y.-K.; Zhang, Z.-J.; Wang, Y.-L.; *et al. Macromol. Chem. Phys.* **2011**, *212*, 81–87.
220. Ritchie, C.; Cooper, G. J. T.; Song, Y.-F.; *et al. Nature Chem.* **2009**, *1*, 47–52.
221. Cooper, G. J. T.; Kitson, P. J.; Winter, R.; *et al. Angew. Chem. Int. Ed.* **2011**, *50*, 10373–10376.
222. Cooper, G. J. T.; Boulay, A. G.; Kitson, P. J.; *et al. J. Am. Chem. Soc.* **2011**, *133*, 5947–5954.
223. Cooper, G. J. T.; Cronin, L. *J. Am. Chem. Soc.* **2009**, *131*, 8368–8369.
224. Parenty, A. D. C.; Smith, L. V.; Pickering, A. L.; *et al. J. Org. Chem.* **2004**, *69*, 5934–5946.
225. Liu, T. B. *Langmuir* **2010**, *26*, 9202–9213.
226. Liu, G.; Liu, T. B.; Mal, S. S.; *et al. J. Am. Chem. Soc.* **2006**, *128*, 10103–10110.
227. Mishra, P. P.; Jing, J.; Francesconi, L. C.; *et al. Langmuir* **2008**, *24*, 9308–9313.
228. Verhoeff, A. A.; Kistler, M. L.; Bhatt, A.; *et al. Phys. Rev. Lett.* **2007**, *99*, 066104.
229. Mishra, P. P.; Pigga, J.; Liu, T. B. *J. Am. Chem. Soc.* **2008**, *130*, 1548–1549.
230. Zhang, J.; Song, Y.-F.; Cronin, L.; *et al. J. Am. Chem. Soc.* **2008**, *130*, 14408–14409.
231. Yan, Y.; Wang, H.; Li, B.; *et al. Angew. Chem. Int. Ed.* **2010**, *49*, 9233–9236.
232. Misdrahi, M. F.; Wang, M.; Pradeep, C. P.; *et al. Langmuir* **2011**, *27*, 9193–9202.
233. Miras, H. N.; Cooper, G. J. T.; Long, D.-L.; Bögge, H.; *et al. Science* **2010**, *327*, 72–74.